

Materials Horizons

Accepted Manuscript

This article can be cited before page numbers have been issued, to do this please use: S. Li, Z. Zhu, Y. Zhang, Y. Liu, X. Zhang and K. N. Hui, *Mater. Horiz.*, 2025, DOI: 10.1039/D5MH00221D.



This is an Accepted Manuscript, which has been through the Royal Society of Chemistry peer review process and has been accepted for publication.

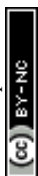
Accepted Manuscripts are published online shortly after acceptance, before technical editing, formatting and proof reading. Using this free service, authors can make their results available to the community, in citable form, before we publish the edited article. We will replace this Accepted Manuscript with the edited and formatted Advance Article as soon as it is available.

You can find more information about Accepted Manuscripts in the [Information for Authors](#).

Please note that technical editing may introduce minor changes to the text and/or graphics, which may alter content. The journal's standard [Terms & Conditions](#) and the [Ethical guidelines](#) still apply. In no event shall the Royal Society of Chemistry be held responsible for any errors or omissions in this Accepted Manuscript or any consequences arising from the use of any information it contains.

Wider Impact Statement

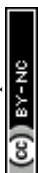
The sustainable production of hydrogen peroxide (H_2O_2) is pivotal for a broad range of industrial and environmental applications, yet its current large-scale synthesis via the anthraquinone process remains energy-intensive and environmentally taxing. This review highlights recent advances in carbon-based electrocatalysts for decentralized, electrochemical H_2O_2 generation—a promising alternative that operates under mild conditions with minimal environmental footprint. The development of efficient, stable, and cost-effective carbon-based materials for electrochemical H_2O_2 production has profound implications for sustainable chemical manufacturing, decentralized wastewater treatment, and green energy applications. By providing a comprehensive analysis of cutting-edge catalyst engineering strategies, mechanistic insights, and structure-performance relationships, this work lays the foundation for the rational design of next-generation carbon-based electrocatalysts. Additionally, this review underscores critical challenges and future research directions, serving as a valuable roadmap for the transition toward scalable, eco-friendly H_2O_2 synthesis. The insights presented herein will not only advance fundamental scientific understanding but also accelerate practical implementation in industrial and environmental sectors.



Data Availability Statement

View Article Online
DOI: 10.1039/D5MH00221D

No new experimental data were generated in this study. All data supporting the findings of this review are available in the cited literature and references within the manuscript.



1 **Innovative Engineering Strategies and Mechanistic Insights for Enhanced**
2 **Carbon-Based Electrocatalysts in Sustainable H₂O₂ Production**

3

4 Shun Li,^{*a} Zhanpeng Zhu,^a Yuqiao Zhang,^a Yong Liu^b, Xinyue Zhang^{*ab} and Kwun Nam
5 Hui^{*c}

6

7 ^a Institute of Quantum and Sustainable Technology (IQST), School of Chemistry and
8 Chemical Engineering, Jiangsu University, Zhenjiang, 212013, China.

9 E-mail: shun@ujs.edu.cn

10 ^b Foshan (Southern China) Institute for New Materials, Foshan, 528200, China.

11 E-mail: zhangxinyue@fscinm.com

12 ^c Joint Key Laboratory of the Ministry of Education, Institute of Applied Physics and Materials
13 Engineering, University of Macau, Avenida da Universidade, Taipa, Macau SAR, China

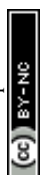
14 E-mail: bizhui@um.edu.mo

15



16 **Abstract:** Hydrogen peroxide (H_2O_2) plays a crucial role in various industrial sectors and
17 everyday applications. Given the energy-intensive nature of the current anthraquinone process
18 for its production, the quest for cost-effective, efficient, and stable catalysts for H_2O_2 synthesis
19 is paramount. A promising sustainable approach lies in small-scale, decentralized
20 electrochemical methods. Carbon nanomaterials have emerged as standout candidates, offering
21 low costs, high surface areas, excellent conductivity, and adjustable electronic properties. This
22 review presents a thorough examination of recent strides in engineering strategies of carbon-
23 based nanomaterials for enhanced electrochemical H_2O_2 generation. It delves into tailored
24 microstructures (e.g., 1D, 2D, porous architectures), defect/surface engineering (e.g., edge sites,
25 heteroatom doping, surface modification), and heterostructure assembly (e.g., semiconductor-
26 carbon composites, single-atom, dual-single-atom catalysts). Moreover, the review explores
27 structure-performance interplays in these carbon electrocatalysts, drawing from advanced
28 experimental analyses and theoretical models to unveil the mechanisms governing selective
29 electrocatalytic H_2O_2 synthesis. Lastly, this review identifies challenges and charts future
30 research avenues to propel carbon electrocatalysts towards greener and more effective H_2O_2
31 production methods.

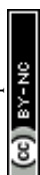
32
33 **Keywords:** Hydrogen peroxide; electrocatalysts; carbon nanomaterials; materials engineering
34



35 1. Introduction

36 Hydrogen peroxide (H_2O_2) is an essential and environmentally friendly chemical with
37 indispensable roles in various industrial applications, including electronics, chemical synthesis,
38 medicine, wastewater treatment, bleaching processes, and environmental remediation.¹⁻⁴
39 Traditionally, industrial H_2O_2 production (~95%) is predominantly achieved through the
40 energy-intensive anthraquinone process,^{5, 6} which involves complex reaction steps, requires
41 toxic solvents under harsh conditions, and generates substantial organic waste, posing
42 significant environmental challenges. These drawbacks have stimulate considerable interest in
43 developing on-site, environmentally benign, energy-efficient, and cost-effective methods for
44 H_2O_2 production, including direct synthesis using H_2 and O_2 ,^{7, 8} photocatalysis,⁹⁻²⁰
45 electrocatalysis,²¹⁻²⁸ mechanocatalysis,²⁹⁻³² and thermoelectrocatalysis.³³⁻³⁵ Among these
46 alternatives, electrochemical synthesis of H_2O_2 is particularly promising because it operates
47 under mild conditions, requiring only electricity, air, and inexpensive electrolytes, while
48 enabling high efficiency and decentralized production.^{36, 37} However, achieving high selectivity
49 for the $2e^-$ reduction pathway to produce H_2O_2 , instead of the $4e^-$ pathway for producing water,
50 is critical for this process.^{38, 39} While noble-metal Pt- and Pd-based alloys have demonstrated
51 excellent performance,^{24, 40, 41} the scarcity and high cost severely limit their practical
52 applications. Therefore, there is increasing interest in developing noble-metal-free
53 electrocatalysts with high-efficiency and selectivity for H_2O_2 production.

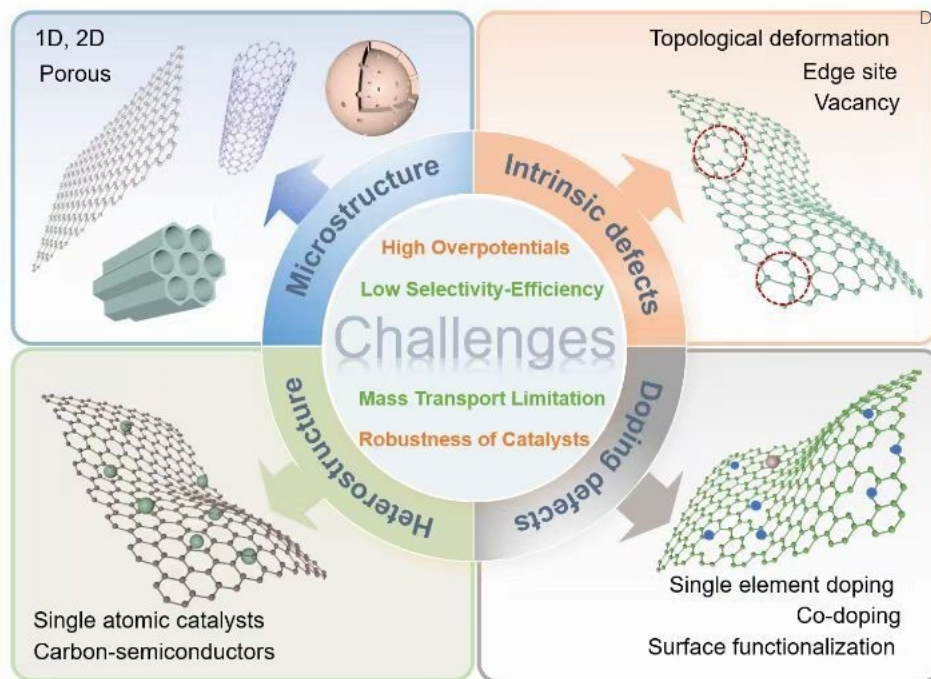
54 Since the pioneering work on nitrogen-doped carbon nanotubes for efficient electrochemical
55 oxygen reduction reaction (ORR) in 2009,⁴² carbon-based metal-free electrocatalysts have
56 garnered considerable research attention.^{43, 44} Various carbon nanomaterials, such as
57 graphene,⁴⁵ carbon nanotubes (CNTs),⁴⁶ carbon nanofibers/wires,⁴⁷ carbon dots,⁴⁸ fullerene,⁴⁹
58 and porous carbon,⁵⁰ have demonstrated great potential as catalysts for electrochemical
59 production of H_2O_2 via $2e^-$ ORR pathway.⁵¹ These materials offer great advantages like low
60 cost, abundant availability, tunable nanostructure, excellent electrical conductivity, and



61 adjustable electronic properties.^{52, 53} However, several challenges remain in optimizing these
62 catalysts for H₂O₂ production, including 1) high overpotential, low catalytic activity and
63 selectivity compared to precious metal catalysts; 2) unclear mechanisms involving active sites
64 and reaction pathways; 3) poor stability and durability in acidic or alkaline environments; 4)
65 integration with electrochemical systems for scalable production.

66 To overcome these inherent limitations, many strategies have been developed in the past few
67 decades. Several important review papers have been published on carbon-based nanomaterials
68 for H₂O₂ production.⁵³⁻⁵⁷ As a rapidly growing field, recent studies have demonstrated notable
69 advancements in the rational design and fabrication of carbon-based electrocatalysts. Moving
70 beyond traditional catalyst optimization methods, innovative engineering strategies have been
71 developed, such as precise modulation of microstructures (e.g., programmed hierarchical
72 structure), multi-component synergistic engineering (e.g., topological and doping effect), and
73 the incorporation of atomically precise catalytic centers (e.g. dual-single-atom sites). These
74 modification strategies have led to significantly enhanced H₂O₂ production activity, selectivity
75 and stability, achieving performance levels that rival or even surpass those of the leading
76 catalysts reported to date. Therefore, it is timely to provide a comprehensive overview of the
77 latest breakthroughs in advanced engineering strategies of carbon-based nanomaterials in
78 electrochemical H₂O₂ production (**Figure 1**). First, we describe the mechanisms of the 2e⁻ ORR
79 and water oxidation reaction (WOR) pathways and elucidate the key factors influencing
80 selectivity and activity. Next, we thoroughly summarize the recent progress in carbon-based
81 electrocatalysts for H₂O₂ synthesis, emphasizing their underlying structure-performance
82 relationships, particularly in the 2e⁻ ORR pathway. Finally, we highlight the current challenges
83 and propose future directions for the rational design and large-scale utilization of advanced
84 carbon-based electrocatalytic materials.





85

86 **Figure 1.** Schematics of key challenges and corresponding modification strategies of carbon-
 87 based electrocatalysts for H_2O_2 production.

88

89 2. Fundamentals of electrochemical H_2O_2 production

90 Electrochemical H_2O_2 production can be achieved through both ORR and WOR (**Figure 2**).

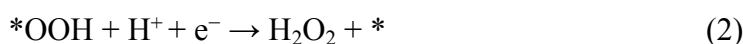
91 These processes involve multi-electron reactions characterized by several elementary steps and
 92 potential intermediates (e.g., $^*\text{OOH}$ and $^*\text{OH}$).^{58, 59} The mechanisms of the ORR and WOR
 93 reactions are presented below in detail.

94 2.1. Two-electron pathway via Oxygen Reduction Reaction (ORR)

95 Generally, ORR involves a complex multi-electron transfer process, which can be
 96 categorized as dissociative and associative mechanisms. For the dissociative mechanism, the
 97 O–O bond in the adsorbed O_2 cleaves directly, resulting in the formation of O_{ads} and H_2O as
 98 the final product. In contrast, the associative mechanism involves the couple of adsorbed O_2
 99 with an electron (e^-) and a proton (H^+) to form the $^*\text{OOH}$ intermediate,⁶⁰ which can further
 100 accept another e^- and H^+ to produce H_2O_2 . Additionally, the O–O bond in the $^*\text{OOH}$
 101 intermediate may also dissociate, yielding O_{ads} and OH_{ads} and ultimately leading to the

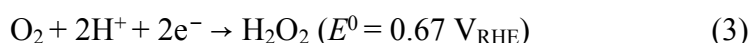


102 formation of H_2O ($^*\text{OOH} + \text{H}^+ + \text{e}^- \rightarrow ^*\text{O} + \text{H}_2\text{O}$).⁶¹ Thus, H_2O_2 is obtained as the main product
 103 by intervening in the dissociation of the peroxide species from the surface, as shown
 104 in Equations 1 and 2.^{62, 63} Thus, the two competitive reactions involving the $^*\text{OOH}$ intermediate
 105 determine the selectivity for H_2O_2 generation.



108 Consequently, ORR mechanisms can be divided into two pathways: the 2e^- or 4e^- pathway.
 109 The 4e^- pathway is preferred as the cathode reaction in fuel cells and metal-air batteries to
 110 obtain higher voltage and energy efficiency, while the electrochemical production of H_2O_2
 111 relies on the 2e^- pathway (Equations 3 and 4).

112 In acidic medium:



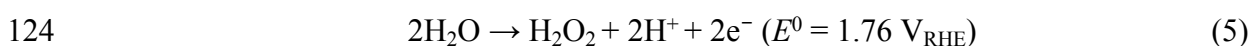
114 In alkaline medium ($\text{pH} > 11.6$):



116 A critical aspect in determining the pathway of the ORR is the adsorption mode of O_2
 117 molecules on the catalyst's surface. In particular, when O_2 is adsorbed in the Pauling mode,
 118 the O–O bond is less likely to break, thus favoring H_2O_2 generation.⁶⁴

119 2.2. Two-electron pathway via Water Oxidation Reaction (WOR)

120 The WOR process can occur through 1e^- , 2e^- , and 4e^- oxidative pathways and H_2O_2 can be
 121 generated via the 2e^- pathway, while the complete oxidation pathway to O_2 needs to be avoided
 122 ($2\text{H}_2\text{O} + 2\text{H}^+ + 2\text{e}^- \rightarrow \text{O}_2$).⁶⁵⁻⁶⁷ The specific WOR steps by 2e^- pathway for H_2O_2 production
 123 are as follows:



View Article Online
DOI: 10.1039/C9/D5MH00221D

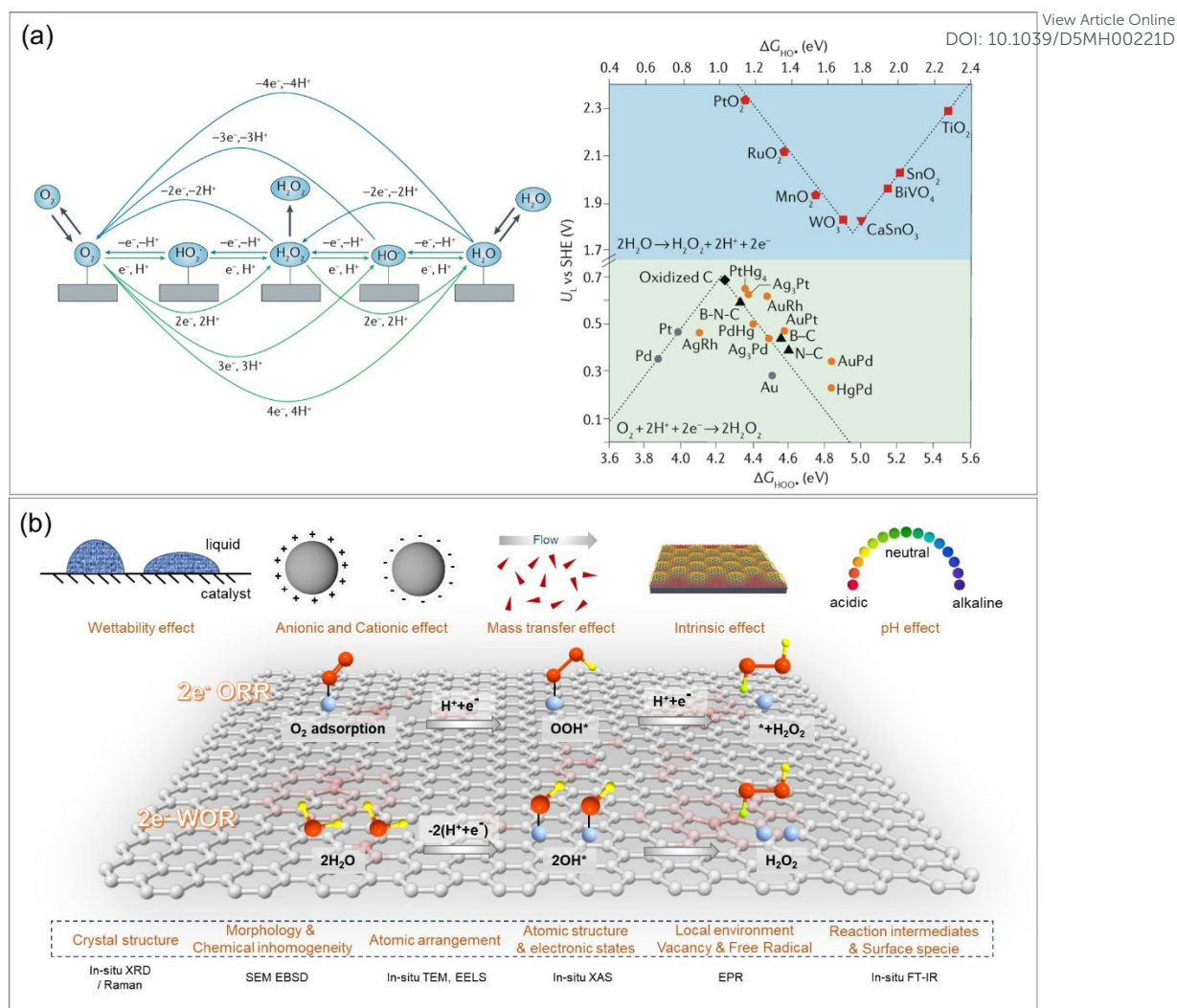
127 The key issue for determining the pathway of the WOR is the recombination of *OH
128 species on the catalyst's surface. Specifically, if *OH is not further oxidized to *O or •OH,
129 H₂O₂ generation is favored.

130 2.3. Mechanistic insights into electrochemical H₂O₂ production

131 In the electrocatalytic production of H₂O₂ via the ORR and WOR mechanisms, the key
132 factors determining efficiency and selectivity mainly include catalyst materials and electrolyte
133 properties. Catalysts with optimized surface electronic structures, such as those exhibiting
134 moderate adsorption energies for oxygen intermediates (e.g., *OOH), favor the 2e⁻ pathway
135 with low overpotential. Additionally, surface properties like porosity, defects, and functional
136 groups can enhance the accessibility of active sites and improve mass transport, further boosting
137 H₂O₂ production. In addition, the electrolyte (e.g., ion type, pH value) also plays a critical role
138 in tuning the reaction kinetics and selectivity. Overall, achieving high activity and selectivity
139 in H₂O₂ electrocatalysis requires a balance modulation of these factors.

140 The electrochemical synthesis of H₂O₂ using carbon-based electrocatalysts involves complex
141 reaction mechanisms that govern their performance in terms of activity, selectivity, and stability.
142 Density functional theory (DFT) calculations (**Figure 2a**) reveal that certain defect
143 configurations in carbon-based materials appear at the pinnacle of the 2e⁻ ORR volcano plot,²
144 highlighting their role as highly active sites. Based on the fundamental mechanisms, key
145 engineering strategies are categorized into: 1) modulation of materials' surface that governs
146 selectivity and mass transfer, 2) reaction pathways and intermediates, and 3) selection of
147 electrolyte. This section provides a cohesive framework for understanding the underlying
148 principles of electrocatalysis H₂O₂ production (**Figure 2b**), which is crucial for optimizing the
149 reactant adsorption/activation, stabilization of intermediates, and efficient product release.





150

151 **Figure 2.** (a) Possible reduction pathways of ORR and WOR for electrocatalysis H_2O_2
 152 production (left) and a plot of theoretical limiting potential (U_L) against Gibbs free energies of
 153 binding $*OOH$ (ΔG_{HOO^*}) and $*OH$ (ΔG_{HO^*}) for H_2O_2 electrocatalysis (right) of different types
 154 of electrocatalysts. U_L is the least positive (anodic) or negative (cathodic) potential at which
 155 both electron transfers are downhill in free energy.² Copyright 2019, Nature Publishing Group.
 156 (b) Schematic illustration of crucial factors and characterization techniques for investigating
 157 the electrocatalytic mechanism.

158

159 2.3.1. Surface properties of electrocatalysts

160 The surface properties of electrocatalysts, where charge and mass transfer of electrochemical
 161 reaction occurs, have crucial effect on the reaction activity.⁶⁸ The surface electronic structure
 162 of electrocatalyst directly determines the adsorption behavior of oxygen-bearing intermediates



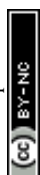
163 (O^* , OH^* , and OOH^*), thereby influencing the activity and selectivity of both the $2e^-$ ORR
164 and WOR. For instance, defect engineering (e.g., edge sites, topological defects, curvature
165 effects, and doping) modulates surface electronic structures and creates active sites to stabilize
166 $*OOH$ and activate O_2 , leading to reduced reaction barriers and favoring the formation of H_2O_2 .
167 In addition, introducing single-atom catalysts on the surface of carbon materials provide precise
168 control over adsorption and binding energies. Microstructure tailoring, such as designing
169 mesoporous hollow nanoreactors, can enhance mass transport and intermediate retention by
170 facilitating O_2 enrichment and H_2O_2 diffusion.

171 Moreover, the wettability of reaction interface, especially hydrophilicity/hydrophobicity,
172 plays an important role in regulating the adsorption/desorption dynamics of products on
173 electrode surface.⁶⁹ For instance, hydrophilic surfaces may facilitate ion transport and reduce
174 gas bubbles overpotential, while controlled hydrophobicity can promote O_2 diffusion to active
175 sites, a crucial factor for the ORR. The balance between hydrophilic and hydrophobic domains
176 can be optimized through chemical functionalization or micro/nanostructuring to create ideal
177 triple-phase boundaries for simultaneous O_2 supply and H_2O_2 release.⁷⁰⁻⁷² When combined with
178 other catalyst modifications (defect engineering, heteroatom doping, etc.), wettability control
179 creates synergistic effects that enhance both the kinetics and thermodynamics of the $2e^-$
180 pathways, bridging fundamental mechanistic understanding with practical catalyst optimization
181 for efficient H_2O_2 production.

182 2.3.2. Reaction pathways and intermediates

183 Both the $2e^-$ ORR and WOR pathways enable selective H_2O_2 production, yet they proceed
184 through fundamentally different reaction mechanisms involving critical intermediates.
185 Theoretical studies have established that the binding energies of ΔG_{OOH^*} and ΔG_{OH^*} serve as
186 main descriptors for catalysts to favour H_2O_2 formation from O_2 or H_2O , respectively.

187 Based on the ORR mechanism, three factors are crucial to ensure high H_2O_2 production
188 selectivity.^{73, 74} Firstly, a suitable O_2 adsorption model is necessary to prevent the dissociative



189 pathway. When the adsorption state is in Pauling mode, the O–O bond is unlikely to break,
190 which is favorable for the generation of H₂O₂. Secondly, the catalysts should balance the strong
191 adsorption of O₂ to facilitate OOH* generation, while allowing moderate desorption to produce
192 H₂O₂ rather than H₂O. Thirdly, it is important to ensure rapid release of the produced H₂O₂
193 from the catalyst surface to avoid further reduction or decomposition.

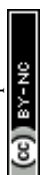
194 As for the WOR process, the selectivity among the 1e⁻, 2e⁻, and 4e⁻ pathways is determined
195 by the descriptors ΔG_{*OH} and ΔG_{*O} , where $\Delta G_{*O} - 2\Delta G_{*OH} = 0.28$ eV.^{75, 76} The selectivity of
196 H₂O₂ production depends on the recombination of two *OH intermediates; If *OH is further
197 oxidized to *O or •OH, the H₂O₂ formation is suppressed. At $\Delta G_{*OH} = 2.38$ eV, *OH can form
198 either H₂O₂ or *O. If the adsorption energy of *O exceeds the production energy of H₂O₂ (3.52
199 eV), the reaction favors the 4e⁻ pathway (with $\Delta G_{*O} < 3.52$ eV and $\Delta G_{*OH} < 1.62$ eV). The
200 optimal condition for the target 2e⁻ WOR occurs when ΔG_{*OH} is between 1.62 and 2.38 eV, as
201 the standard potential is more positive than that of H₂O₂ oxidation ($E^0 = 0.67$ V_{RHE}).

202 2.3.3. Role of electrolyte

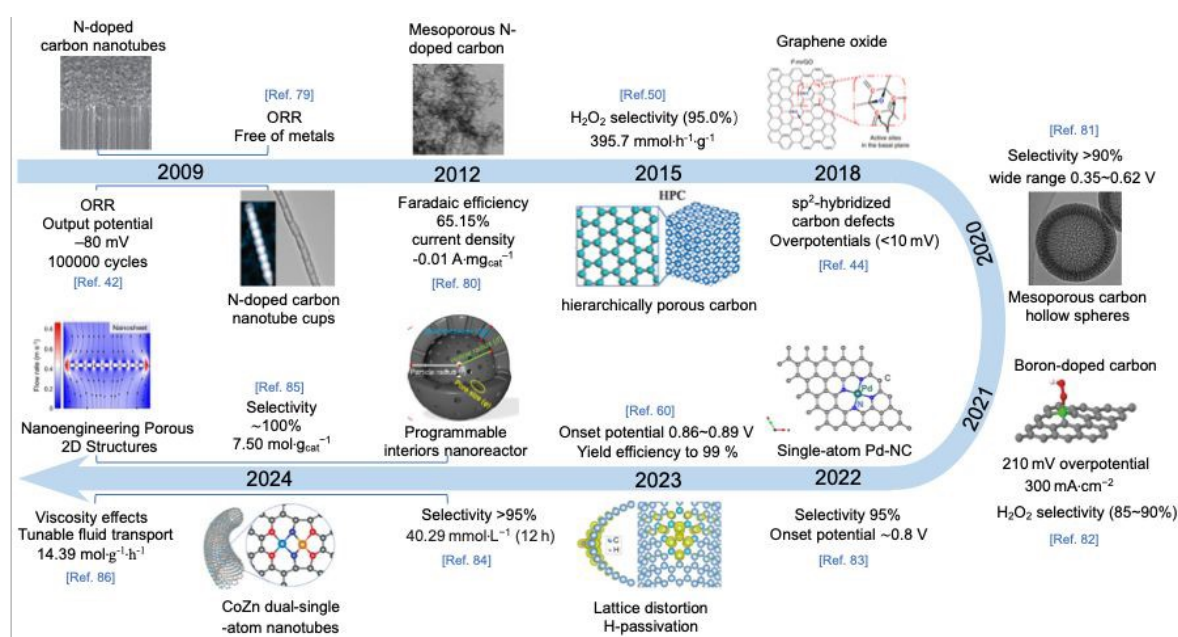
203 The electrolyte is also critical in electrochemical H₂O₂ production process, particularly when
204 pairing 2e⁻ ORR and 2e⁻ WOR in traditional liquid electrolytes ranging from acidic to alkaline
205 pH. For 2e⁻ ORR, the pH of electrolyte affects the selectivity due to the solvation effects and
206 surface adsorbed species (such as *OH_{ads} and anions).^{22, 77} In alkaline medium, the •OH species
207 are strongly adsorbed on the catalyst surface, facilitating outer-sphere electron transfer via
208 water-solvated molecular O₂. In contrast, acidic electrolytes promote high proton mobility,
209 resulting in low concentrations of adsorbed •OH species. Here, O₂ molecules are chemisorbed
210 on the catalyst surface, receiving electrons through the inner-Helmholtz plane (IHP) process.⁷⁸

211 3. Engineering strategies for carbon-based electrocatalysts

212 The catalytic performance of materials is intrinsically determined by the physicochemical
213 properties of their surfaces, which govern the adsorption and desorption of reactive species and
214 influence key parameters such as activity, selectivity, and stability. Pristine carbon materials



215 often suffer from low catalytic activity and poor selectivity due to their relatively inert surfaces
 216 and limited active sites. To overcome these inherent limitations, a range of advanced
 217 engineering strategies have been developed, including microstructure design, defect
 218 engineering, chemical doping, surface functionalization, and introduction of heterojunction or
 219 atomic sites, to enhance the electrocatalytic performance of carbon nano-catalysts toward H₂O₂
 220 production, primarily focusing on the 2e⁻ ORR pathway. The roadmap of carbon-based
 221 electrocatalysts illustrating the key findings is summarized in **Figure 3**.



222
 223 **Figure 3.** Timeline of engineering strategies for carbon-based electrocatalysts for H₂O₂
 224 production: N-doped carbon nanotubes,⁴² reduced graphene oxide,⁴⁴ hierarchically porous
 225 carbon,⁵⁰ N-doped carbon nanotubes cups,⁷⁹ mesoporous N-doped carbon,⁸⁰ Mesoporous
 226 carbon hollow spheres,⁸¹ boron-doped carbon,⁸² single-atom Pd/carbon,⁸³ Lattice distortion
 227 Carbon,⁶⁰ mesoporous carbon spheres,⁸⁴ CoZn dual-single-atom carbon nanotubes,⁸⁵ and
 228 porous 2D structures.⁸⁶

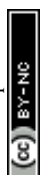
229 3.1. Microstructure tailoring

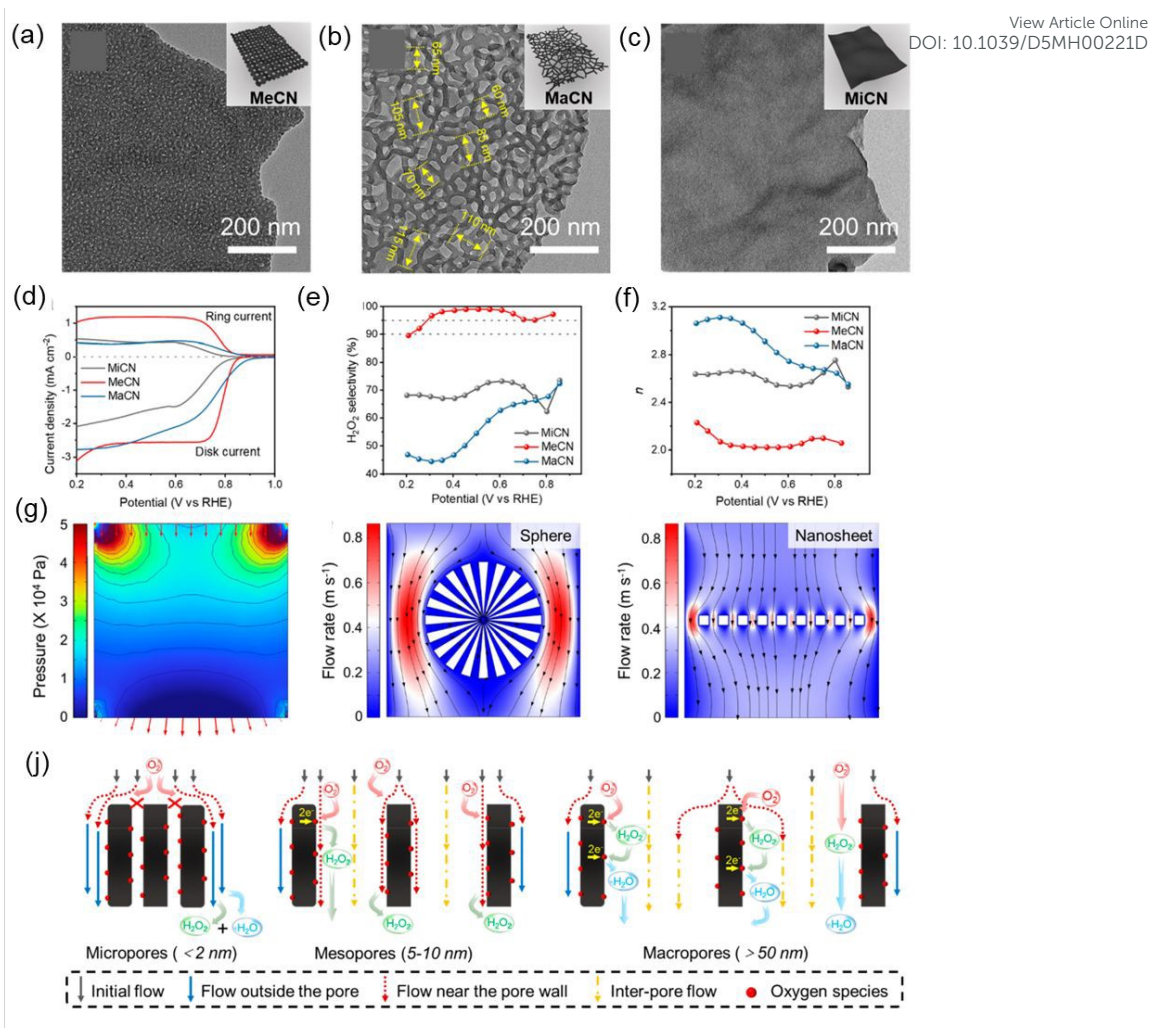
230 Modifying the microstructure of carbon materials plays a vital role in boosting their catalytic
 231 performance. Constructing various nanostructures, such as 1D (e.g., nanotube and nanorods),
 232 2D (e.g., graphene), porous architectures (e.g., macropores, mesopores and micropores), and
 233 hierarchical structures, leads to significant improvements in surface area, exposure of active



234 sites, mass diffusion, and electrical conductivity. These enhanced properties are crucial for
235 increasing the efficiency and selectivity of the catalyst during the electrocatalysis process.

236 The catalytic performance of microstructures is heavily influenced by their dimensions and
237 porosity, as these factors determine the accessibility of active sites and the transport of reactants
238 and products.^{87, 88} For example, 1D nanostructures such as nanotubes provide excellent electron
239 transport pathways, while 2D nanostructures like graphene sheets offer high surface areas for
240 active site exposure. Moreover, when porous architectures are introduced, such as macropores
241 (larger pores that facilitate mass transport), mesopores (intermediate-sized pores that enhance
242 exposure of active sites), and micropores (smaller pores that control the retention of reactants),
243 the material's ability to regulate reaction intermediates and diffusion kinetics can be greatly
244 promoted.⁸⁹ Moreover, the $2e^-$ ORR can be regulated by controllable pore structures through
245 adjusting the coordination of reaction intermediates. By optimizing the exposure of active sites
246 and retention time of H_2O_2 within specialized pore sizes, the overall performance of the catalyst
247 can be finely tuned.^{51, 90} Recently, hollow structures that typically feature lower density and
248 larger surface area, have garnered significant attention due to their unique properties compared
249 to solid counterparts, by facilitating mass transport and enhancing the availability of active sites.
250 The increased surface-to-volume ratio in hollow structures further contributes to higher
251 utilization of the catalyst material, making them highly attractive for electrocatalytic H_2O_2
252 production.^{81, 91-93} This section will mainly focus on the key latest advances in the rational
253 design of high efficient carbon-based electrocatalysts with controllable microstructures.



View Article Online
DOI: 10.1039/D5MH00221D

254

255 **Figure 4.** Nanoengineering of porous 2D carbon structures for ORR H_2O_2 production. TEM
 256 images and structural models of (a) MeCN, (b) MaCN, and (c) MiCN; (d) LSV curves recorded
 257 in an O_2 -saturated KOH, (e) calculated H_2O_2 selectivity, and (f) ORR electron transfer number
 258 at various potentials; (g) Color mapping of the spatial pressure distribution, and spatial
 259 distribution of flow velocities of the mesoporous carbon sphere and nanosheet model (pore size:
 260 5 nm); (j) Proposed fluid behavior and ORR processes in micropores, mesopores, and
 261 macropores. Reproduced with permission.⁸⁶ Copyright 2024, the American Chemical Society.
 262

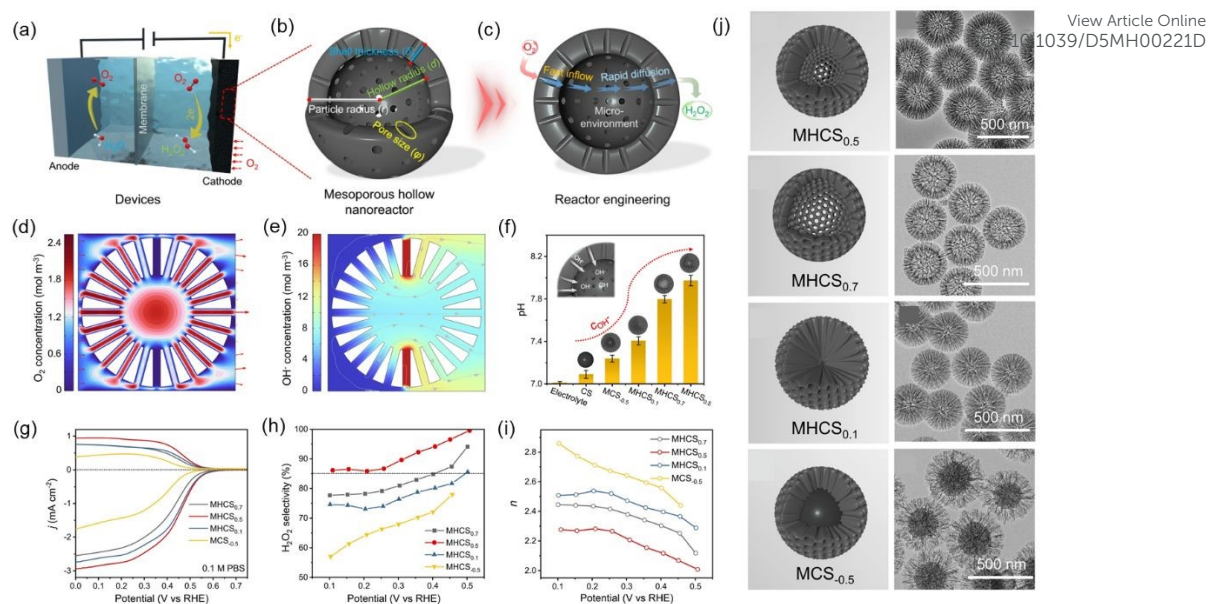
263 Precision nanoengineering of porous 2D structures has been emerging as a promising strategy
 264 for fine-tuning catalytic reactions. Guided by finite element simulations (FEM), Tian *et al.*⁸⁶
 265 designed and fabricated porous 2D carbon nanomaterials by introducing mesopores with
 266 diameters of 5–10 nm to facilitate fluid acceleration (**Figure 4a-c**). The resulting mesoporous
 267 carbon nanosheets exhibited exceptional electrocatalytic H_2O_2 production performance,
 268 achieving a high selectivity of >95% and a diffusion-limiting disk current density of -3.1 mA
 269 cm^{-2} (**Figure 4d-f**). FEM simulations revealed that the mesoporous nanosheet significantly



270 accelerated fluid flow within the meso-channels due to viscosity effects and the constricted flow
271 path (**Figure 4g**), validating the crucial role of mesoporous 2D structures in enhancing local
272 diffusion. Remarkably, the electrolysis process in a flow cell achieved a high production rate
273 of 14390 mmol g⁻¹ h⁻¹, yielding a medical-grade H₂O₂ solution. This work demonstrates an
274 effective approach to improving the activity and selectivity of porous carbon materials by
275 influencing local fluid transport behavior.

276 Mesoporous hollow nanoreactors (MHNs), a novel class of rationally designed catalytic
277 material, offer unique advantages of complex catalytic processes due to their hollow internal
278 spaces and mesoporous structures.⁹⁴⁻⁹⁶ The mesoporous channels can create a confined
279 microenvironment that enhances molecular diffusion, adsorption and surface reactions,
280 enabling tunable catalytic pathways. For instance, Tian *et al.*⁸⁴ demonstrated precisely
281 engineered carbon spheres by integrating micromechanics with controllable synthesis to
282 improve their 2e⁻ ORR catalytic activity (**Figure 5**). The mesoporous channels accelerated fluid
283 flow and facilitated the transport of generated H₂O₂ into the solution (**Figure 5a-c**), thereby
284 minimizing electro-reduction on the catalysts' surface. Increased flow rates led to O₂
285 enrichment in the pore channels (**Figure 5d**), while the accumulation of OH⁻ ions (**Figure 5e**)
286 elevated the local pH within the MHNs. And the surface of MHCS_{0.5} electrode demonstrated
287 the highest OH⁻ concentrations among all samples (**Figure 5f**). As a result, MHCS_{0.5} exhibited
288 exceptional 2e⁻ ORR performance in neutral electrolyte conditions (pH = 7), with a diffusion-
289 limited disk current of -2.8 mA cm⁻² at 0.2 V an onset potential of 0.6 V (vs. RHE), and an
290 H₂O₂ selectivity exceeding 85%, outperforming most carbon-based catalysts reported in the
291 literature.



View Article Online
1039/D5MH00221D

292

293 **Figure 5.** Nanoreactor design based on carbon nanospheres. (a-c) Schematic diagram for
 294 electrochemical $2e^-$ ORR to produce H_2O_2 over the designed nanoreactor; Spatial distribution
 295 of (d) O_2 and (e) OH^- concentration in the mesoporous carbon sphere model;
 296 (f) OH^- concentrations on the surface of $MHCS_x$; (g) LSV curves of RRDE measurements, (e)
 297 H_2O_2 selectivity, and (i) electron transfer number at various applied potentials; (j) Structural
 298 model and TEM images of $MHCS_x$. Reproduced with permission.⁸⁴ Copyright 2024, Nature
 299 Publishing Group.

300

301 3.2. Defect engineering

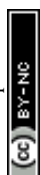
302 Defects in carbon nanomaterials, such as vacancies, rings, edge sites, topological defects,
 303 and lattice distortion, play a crucial role in modulating their electronic structure and surface
 304 chemistry. Introducing structural defects can generate abundant active sites that enhance the
 305 adsorption and activation of oxygen molecules, thereby improving the selectivity and efficiency
 306 of the ORR towards H_2O_2 production.^{97,98} For instance, vacancies provide more exposed active
 307 sites, while edge defects create abundant unsaturated bonds.⁹⁹ Beyond enhancing catalytic
 308 reactivity, defect engineering could also improve the durability and stability of the
 309 electrochemical system, making it more suitable for industrial applications.⁹⁷ In the past decade,
 310 significant efforts have been made to explore defective carbon catalysts for electrochemical
 311 H_2O_2 production.¹⁰⁰⁻¹⁰⁴ In this section, we will highlight the key advances in defect engineering

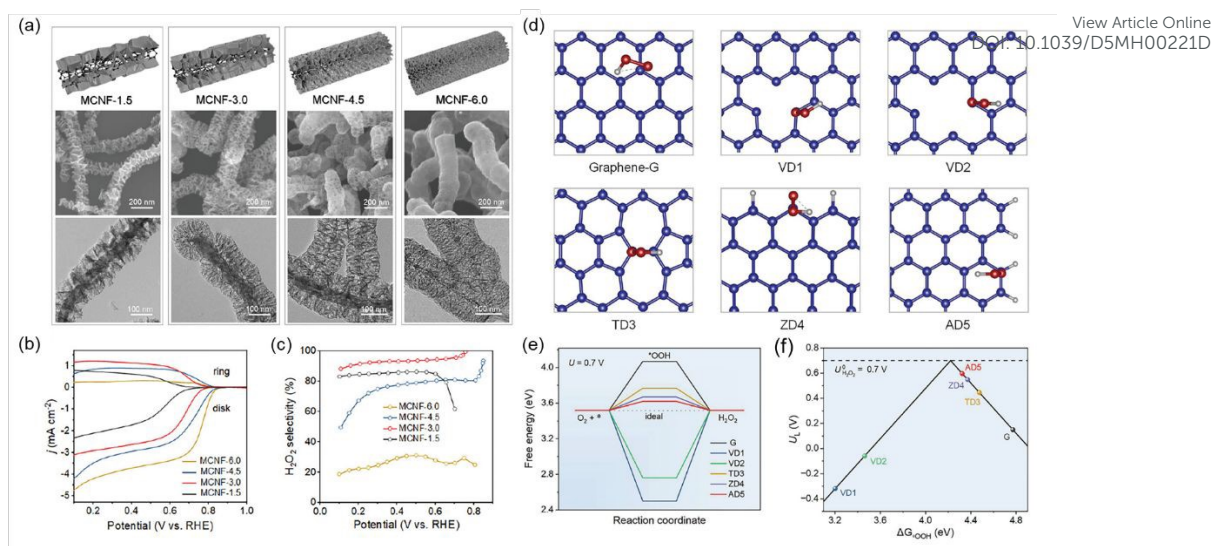


312 of carbon electrocatalyst including both intrinsic defects (e.g., edge defects, topological defects)
313 and chemical doping with heteroatoms (e.g., single element and dual-elements doping).

314 3.2.1 Intrinsic defects

315 Edge engineering has emerged as a promising strategy to activate inert carbon surfaces and
316 modify their local electronic structure by introducing unpaired electrons.^{105, 106} For example,
317 Jing *et al.*⁹⁹ developed an organic-inorganic hybrid co-assembly approach to fabricate
318 mesoporous carbon nanofibers (MCNFs) with tunable edge site densities and pore sizes, using
319 ammonia to catalyze the modular molding of SiO₂ and resin (**Figure 6a**). They demonstrate that
320 the density of carbon edge sites can be controlled to enhance ORR activity and selectivity. The
321 optimized MCNFs catalyst exhibited outstanding 2e⁻ ORR performance (**Figure 6b** and **c**),
322 achieving high H₂O₂ selectivity (>90%) over a wide potential range of 0.6 V, along with a large
323 cathodic current density of -3.0 mA cm⁻² at 0.2 V vs. RHE. As illustrated in **Figure 6d**, the
324 defect configurations comprised vacancies (VD1 and VD2), topological defects (TD3), and
325 edge defects, including zigzag and armchair types (ZD4 and AD5, respectively). The
326 introduction of these defects enhanced *OOH adsorption, with the zigzag defect (ZD4) and
327 armchair (AD5) defects exhibiting free energies of 3.67 and 3.62 eV, respectively, values close
328 to the ideal standard free energy of 3.52 eV (**Figure 6e** and **f**). These results demonstrate that
329 edge defects can effectively promote the 2e⁻ ORR pathway, offering a promising route to
330 achieving high H₂O₂ production activity selectivity in carbon-based electrocatalysts.



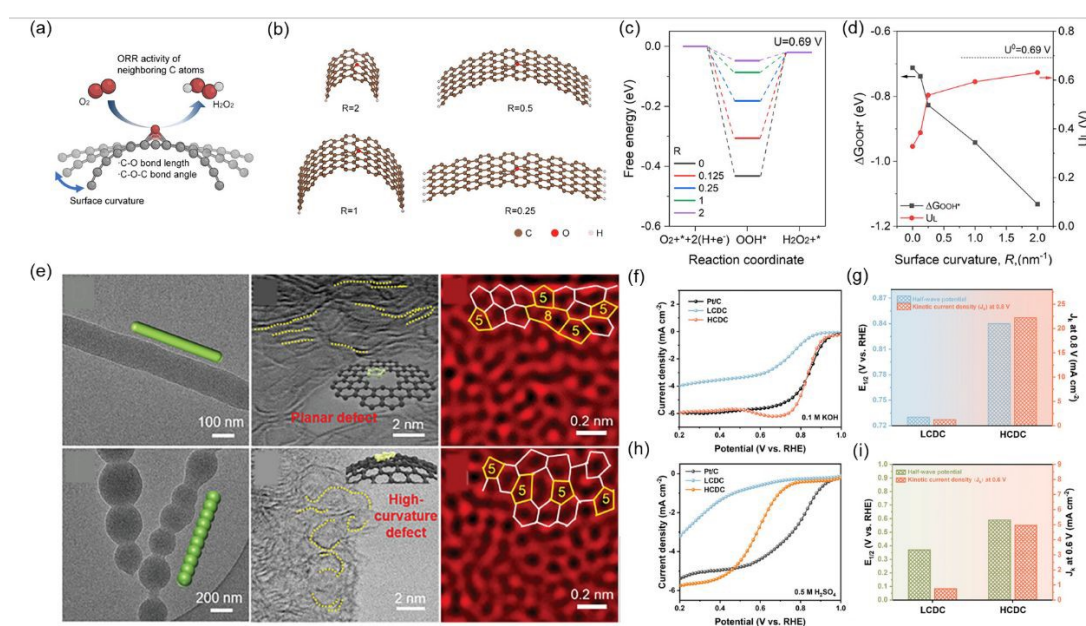
View Article Online
DOI: 10.1039/D5MH00221D

331
332 **Figure 6.** Edge defect engineering of ORR activity. (a) Schematic, SEM, and TEM images of
333 different mesoporous carbon nanofibers (MCNFs); (b) LSV curves and (c) calculated H_2O_2
334 selectivity; (d) Preferred *OOH adsorption configurations on pristine graphene and different
335 carbon defects models (blue, grey, and red represent C, H, and O atoms, respectively); (e) Free-
336 energy profiles of ORR paths at potential of 0.7 V; (f) Volcano plot for the most active structures,
337 with the limiting potential depicted as a function of $\Delta G_{\text{*OOH}}$. Reproduced with permission.⁹⁹
338 Copyright 2023, Wiley-VCH.

340 By introducing asymmetric structures into hexagonal carbon lattice, the symmetry can be
341 broken to allow rapid electron transfer, thus promoting the electrocatalytic process. Recently,
342 topological defects have been recognized as effective active sites toward catalyzing different
343 electrochemical reactions. She *et al.*¹⁰⁷ investigated the curvature-dependent ORR activity of
344 surface oxidized carbon nanotubes (o-CNTs) (**Figure 7a-d**). Computation modeling suggested
345 that the curvature can alter epoxy group geometry, exerting greater strain on the C–O bond in
346 smaller diameter o-CNTs that leads to improved activity. Increase of R results in stronger
347 OOH^* binding and a lower ΔG_{OOH^*} (**Figure 7c**), and 2e-ORR theoretical potential (U_L)
348 approaches the equilibrium potential ($E^0 = 0.69$ V) on a model with a greater R (**Figure 7d**). As
349 predicted, the o-CNT with the smallest diameter (~ 8 nm) exhibited the highest Faradaic
350 efficiency $>85\%$ and a mass activity of 161 A g^{-1} at 0.65 V. Very recently, Wang *et al.*¹⁰⁸
351 fabricated carbon nanomaterials with rich topological defect sites and curved defective surface
352 by controlling the pyrolytic shrinkage process of precursors (**Figure 7e-i**). Theoretical



353 calculations demonstrated that bending the defect sites can manipulate the local electronic
 354 structure, facilitate the charge transfer to key intermediates, and reduce the ORR energy barrier.
 355 Experimental results showed that a large kinetic current density of 22.5 mA cm^{-2} at 0.8 V vs.
 356 RHE was obtained for high-curvature defective carbon (HCDC), which is ~ 18 times of low-
 357 curvature defective carbon (LCDC). Further increasing the defect densities of HCDC results in
 358 a dual-regulated product (HCHDC), which exhibited exceptional ORR activity in both alkaline
 359 and acidic media (half-wave potentials of 0.88 and 0.74 V , respectively), exceeding most of the
 360 reported carbon electrocatalysts. These studies highlight the crucial role of curvature effect in
 361 promoting electrocatalytic activity and offer new guidance to the design of advanced carbon
 362 nano-catalysts for H_2O_2 production.



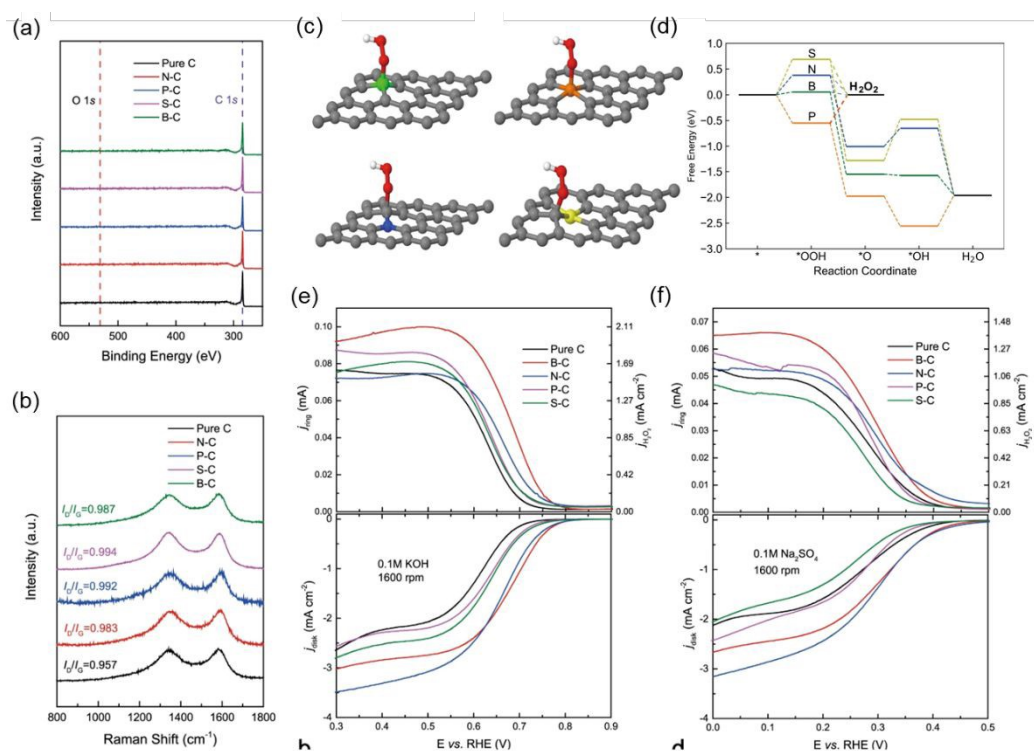
363
 364 **Figure 7.** Investigation of the curvature-dependent ORR activity. (a) Schematic illustration of
 365 the epoxy group grafted on curvature varied carbon surface and (b) geometry optimized atomic
 366 models of different R values; (c) Calculated ORR free energy diagrams at 0.69 V and (d)
 367 correlations between ΔG_{OOH^*} and U_L to surface curvature. Reproduced with permission.¹⁰⁷
 368 Copyright 2024, the American Chemical Society. (e) TEM, HRTRM, and AC HAADF-STEM
 369 images of LCDC and HCDC (insets are morphology and atomic structure diagrams); (f) LSV
 370 curves in O_2 -saturated KOH and (g) comparison of J_k (0.8 V) and $E_{1/2}$; (h) LSV curves of
 371 LCDC, HCDC, and Pt/C in O_2 -saturated H_2SO_4 and (i) comparison of J_k (0.6 V) and $E_{1/2}$.
 372 Reproduced with permission.¹⁰⁸ Copyright 2024, Wiley-VCH.

373

374 3.2.2 Heteroatom doping



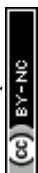
375 Incorporating non-metallic/metallic heteroatoms, such as boron (B),¹⁰⁹⁻¹¹¹ nitrogen (N),¹⁰³
 376 ¹¹² oxygen (O),^{113, 114} fluorine (F),¹¹³ and sulfur (S),¹¹⁵ into the carbon lattice can disturb the
 377 electron symmetry in the aromatic carbon networks, providing the inhomogeneous
 378 compositions and active sites by means of tailoring the charge and spin densities of carbon
 379 atoms. In addition, heteroatoms could introduce active functional groups (oxygen-bearing
 380 functional groups) onto the carbon matrix, which can serve as active sites for 2e⁻ ORR, to
 381 achieve high electrocatalysis activity. Up till now, extensive studies have been reported on this
 382 strategy, herein we only summarize the latest achievements on heteroatom doping to enhance
 383 electrocatalytic H₂O₂ generation activity.



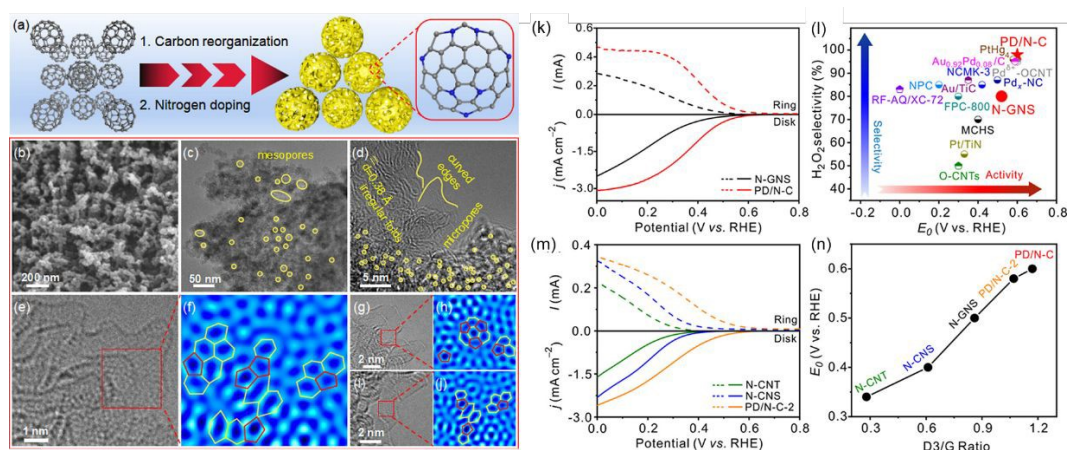
384

385 **Figure 8.** Heteroatom-doped carbon catalysts for electrocatalytic H₂O₂ generation. (a) XPS
 386 survey scan and (b) Raman spectroscopy for pure C and B, N, P, S-doped carbon catalysts; (c)
 387 Preferred *OOH adsorption configurations on B-, P-, N-, and S-doped graphene, respectively.
 388 Green, orange, blue, yellow, gray, red, and white spheres represent B, P, N, S, C, O and H,
 389 respectively; (d) Free-energy profile of O₂ reduction paths ($U_{\text{RHE}} = 0.7 \text{ V}$); LSV curves and
 390 H₂O₂ currents (1.2 V vs. RHE) recorded by RRDE in (e) 0.1M KOH and (f) 0.1M Na₂SO₄.
 391 Reproduced with permission.⁸² Copyright 2021, Nature Publishing Group.

392



393 In 2021, Xia *et al.*⁸² reported a boron-doped carbon (B-C) catalyst (**Figure 8**). Compared to
 394 the state-of-the-art oxidized carbon catalyst, the B-C catalyst presented significantly lowered
 395 overpotential by 210 mV under industrial-level currents (300 mA cm^{-2}) while maintaining high
 396 H_2O_2 selectivity (85–90%) (**Figure 8e** and **f**). DFT calculations revealed that the boron dopant
 397 site is responsible for high H_2O_2 activity and selectivity due to the reduced thermodynamic and
 398 kinetic reaction barriers (**Figure 8c** and **d**). Integrated in a porous solid electrolyte reactor, the
 399 B-C catalyst demonstrated continuous generation of pure H_2O_2 solutions with high a current
 400 density ($\sim 400 \text{ mA cm}^{-2}$) and selectivity ($\sim 95\%$), presenting their great potential for practical
 401 applications in the future.



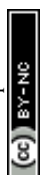
402
 403 **Figure 9.** Pentagonal defect-rich N-doped carbon nanomaterial (PD/N-C) using fullerene (C_{60}).
 404 (a) Schematic of the synthesis of PD/N-C; (b) SEM, (c,d) TEM, and (e,g,i) AC-STEM images
 405 and (f,h,j) the corresponding Fourier transform fitting results of PD/N-C; (k) RRDE
 406 polarization curves and H_2O_2 currents at the ring electrode of PD/N-C and N-GNS; (l)
 407 Comparison of $2e^-$ ORR performance of representative electrocatalysts; (m) RRDE
 408 polarization curves and H_2O_2 currents at the ring electrode of N-CNT, N-CNS, and PD/N-C-2;
 409 (n) Onset potential (E_0) as a function of the D3/G ratio of a series of samples. Reproduced with
 410 permission.¹⁰³ Copyright 2023, the American Chemical Society.

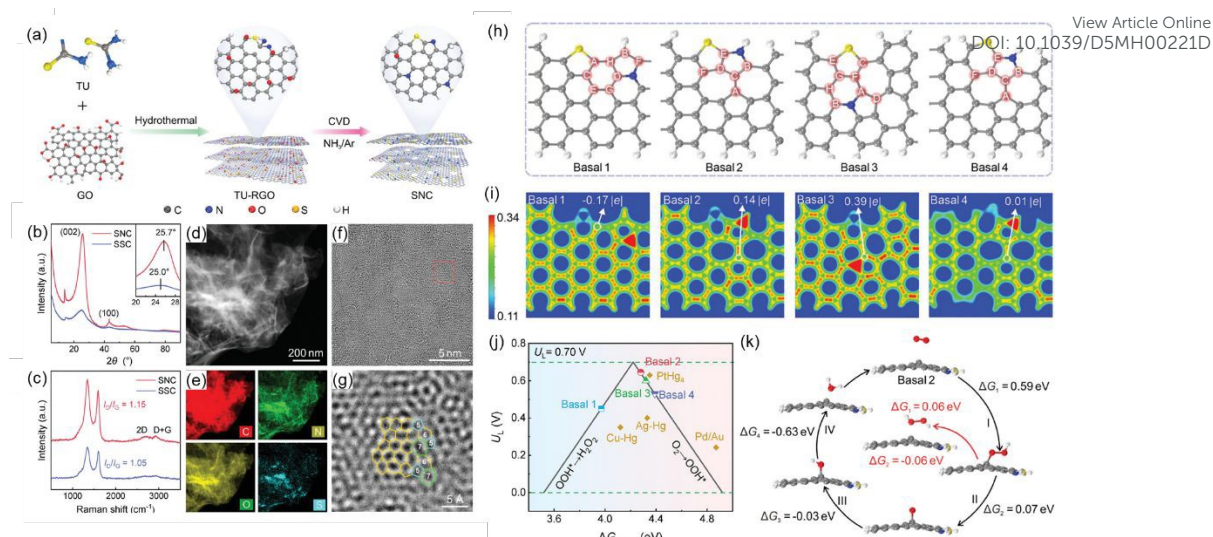
411
 412 Oxygen-doped carbon quantum dots (o-CQD) with C–O–C surface functional groups was
 413 fabricated with tunable electronic structure by varying isomerization precursors,¹¹⁴ presenting
 414 a remarkable H_2O_2 selectivity of 96.2% ($n = 2.07$) at 0.68 V vs. RHE along with a low Tafel
 415 slope of $66.95 \text{ mV dec}^{-1}$, and maintaining consistent production stability of H_2O_2 over 120 h.
 416 In addition, hierarchical porous boron-doped carbon (B-DC) electrocatalyst was synthesized



417 from fullerene (C_{60}) frameworks and boric oxide.¹⁰⁹ Benefitting from boron doping and abundant
418 topological pentagon defects, the B-DC catalysts exhibited a high ORR onset potential of 0.78
419 V and a $2e^-$ selectivity over 95%. Remarkably, the B-DC electrocatalyst-based device achieved
420 a remarkable H_2O_2 yield rate of $247 \text{ mg} \cdot \text{L}^{-1} \cdot \text{h}^{-1}$ and quantitative Faraday efficiency of nearly
421 100%. For sulfur-doped defective nanocarbons (S-DNC), a similar high ORR onset potential
422 (0.78 V) and selectivity (90%) was obtained, with an superior H_2O_2 yield rate of $690 \text{ mg L}^{-1} \text{ h}^{-1}$
423 in a H cell.¹¹⁵ In 2023, Lu *et al.*¹⁰³ designed and fabricated a pentagonal defect-rich N-doped
424 carbon nanomaterial (PD/N-C) via pyrolysis of C_{60} as the precursor followed by ammonia
425 treatment (**Figure 9a**). A great number of mesopores and micropores were created in PD/N-C,
426 along with abundant irregular folds and curved edges (**Figure 9b–d**). Moreover, the aberration-
427 corrected scanning TEM (AC-STEM) and the corresponding fitting results (**Figure 9e–j**)
428 further demonstrate that the PD/N-C sample contains rich pentagon defects. As a result, the
429 PD/N-C catalysts achieved excellent $2e^-$ ORR activity, selectivity, and stability in acidic
430 electrolytes, even outperforming the Pt-Hg alloy catalyst. The linear sweep voltammetry curves
431 (**Figure 9k**) show that the PD/N-C catalyst achieves a larger ORR current density (3.1 mA cm^{-2}
432 at 0 V) along with a higher onset potential in a wide potential range from 0 to 0.6 V, as
433 compared to N-doped carbon nanomaterial dominated by hexagons graphene nanosheets (N-
434 GNS). This performance is among the top of all reported metal-free carbon-based catalysts and
435 even superior to some noble-metal-based catalysts and the benchmark PtHg_4 alloy catalyst in
436 acidic electrolytes (**Figure 9l**). By comparing a series of samples, the synergetic effects of both
437 topological defects and N-doping are responsible for the superb $2e^-$ ORR performance of the
438 PD/N-C catalysts (**Figure 9m and n**).

View Article Online
DOI: 10.1039/D5MH00221D





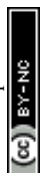
439

440 **Figure 10.** Pentagon-S and pyrrolic-N coordinated (SNC) graphene with in-plane topological
 441 defects. (a) Schematic illustration of synthesis for graphene pentagon-S and pyrrolic-N
 442 coordinated (SNC); (b-g) XRD patterns, Raman spectra, TEM images, and EDS mappings; (h)
 443 Computational models, (i) Bader charge, (j) activity-volcano plot ($U_L = 0.70$ V), and (k) ORR
 444 reaction pathway diagrams and corresponding energy barriers for each step on Basal 2.
 445 Reproduced with permission.¹⁰⁰ Copyright 2024, Wiley-VCH.

446

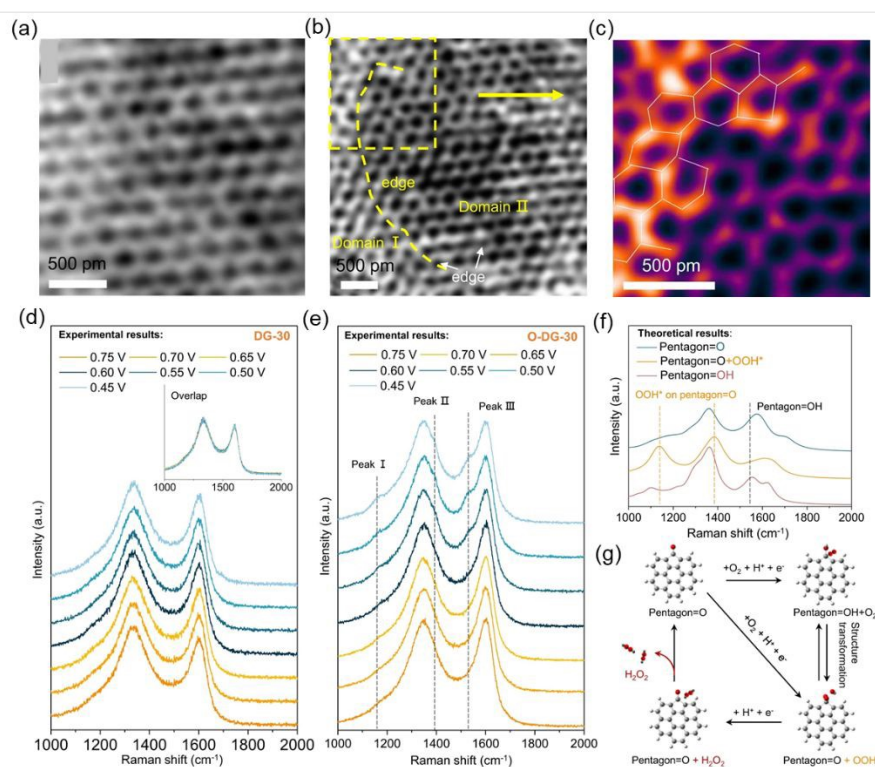
447

448 In addition to single-element doping, dual elements co-doping on carbon materials have been
 449 received increasing research attention toward electrocatalytic $2e^-$ ORR due to the unique
 450 synergistic effect.¹¹⁶ For instance, a yolk-shell B/N co-doped hollow carbon nanosphere, with
 451 oxygen-vacancy decorated reduced graphene oxide coating (B/N-HCNS@VO-G) was reported
 452 as an efficient metal-free electrocatalyst for $2e^-$ ORR with high durability.¹¹⁷ Such a dual-
 453 doping electrocatalyst leads to excellent electrocatalytic H_2O_2 production performance with a
 454 high selectivity of 91% and yield of 56 ppm (0.7 V), allowing in-situ antibiotic and dye
 455 degradation for on-site wastewater remediation. Very recently, pentagon-S and pyrrolic-N
 456 coordinated (SNC) graphene with in-plane topological defects was synthesized through a two-
 457 step hydrothermal and nitridation procedure (**Figure 10**).¹⁰⁰ The SNC is composed of stained
 458 hexagons with sporadic pentagons (**Figure 10d-g**), suggesting that the hexagonal topological
 459 structure of the carbon matrix is significantly distorted. In addition, the dual-doping of S and N
 460 elements introduces unsymmetrical dumbbell-like S–C–N motifs, which can effectively tune
 the electronic structures of graphene (**Figure 10h** and i). Theoretical calculations further



461 unveiled that the defective S–C–N motifs can effectively optimize the binding strength to
 462 OOH* intermediate and reduce the energy barrier for ORR to H₂O₂ (**Figure 10j**). As a result,
 463 the SNC catalyst exhibited ultrahigh H₂O₂ production rate of 8100, 7300, and 3900 mmol
 464 g⁻¹ h⁻¹ in alkaline, neutral, and acidic electrolytes, respectively.

465 It is worth mentioning that doping with heteroatoms into carbon matrix could also induce
 466 surface functional groups. For example, oxygen functionalization onto the parent carbon
 467 structures has been reported to be effective to improve 2e⁻ ORR performance.^{21, 118, 119} For
 468 instance, oxygen-doped carbon dots (O-CDs) was synthesized by solvent engineering approach
 469 and exhibited excellent catalytic activity.¹²⁰ By tuning the ratio of ethanol and acetone solvents
 470 during the synthesis, the surface electronic structure of the resulting O-CDs can be precisely
 471 modulated. The selectivity and activity of the O-CDs was strongly dependent on the amount of
 472 edge active C–O groups, achieving the highest H₂O₂ selectivity up to ~96.6% (*n* = 2.06, 0.65 V
 473 vs. RHE) and an ultralow Tafel plot of 64.8 mV dec⁻¹.



474

475 **Figure 11.** In-situ investigation of dynamic active site in oxygen modified defective graphene
 476 (O-DG) electrocatalysts. iDPC-STEM image of O-DG-30 in (a) perfect domain and (b and c)



477 defective domain; In-situ Raman spectra of (d) DG-30 and (e) O-DG-30 on flow cell in O₂-
478 saturated 0.1 M KOH; (f) The calculated Raman spectra of three possible atomic structures of
479 the O-groups and relevant surface species on defective graphene; (g) Schematic diagram of
480 possible electrocatalytic mechanism of O-DG. Reproduced with permission.¹²¹ Copyright 2023,
481 Nature Publishing Group.

482
483 Despite tremendous works on doped carbon materials for electrocatalysis H₂O₂ production,
484 the dynamic structural transformation of these materials during electrocatalysis reaction process
485 has been received less attention. Active sites identification in carbon materials is crucial for
486 understanding the mechanism, but resolving precise configuration of active site remains a huge
487 challenge. In 2023, Wu *et al.*¹²¹ manipulated the defect density and oxygen groups on graphene,
488 and revealed the oxygen groups redistribution and positive correlation relationship between the
489 defect density and their ORR performance (**Figure 11**). The dynamic evolution processes of
490 defects were monitored through in-situ Raman, FTIR and XPS technologies, combined with
491 theoretical simulations. The results clarified the configuration of major active sites (carbonyl
492 on pentagon defect) and key intermediates (*OOH), providing deep understanding of the
493 catalytic mechanism for doped defective carbon materials.

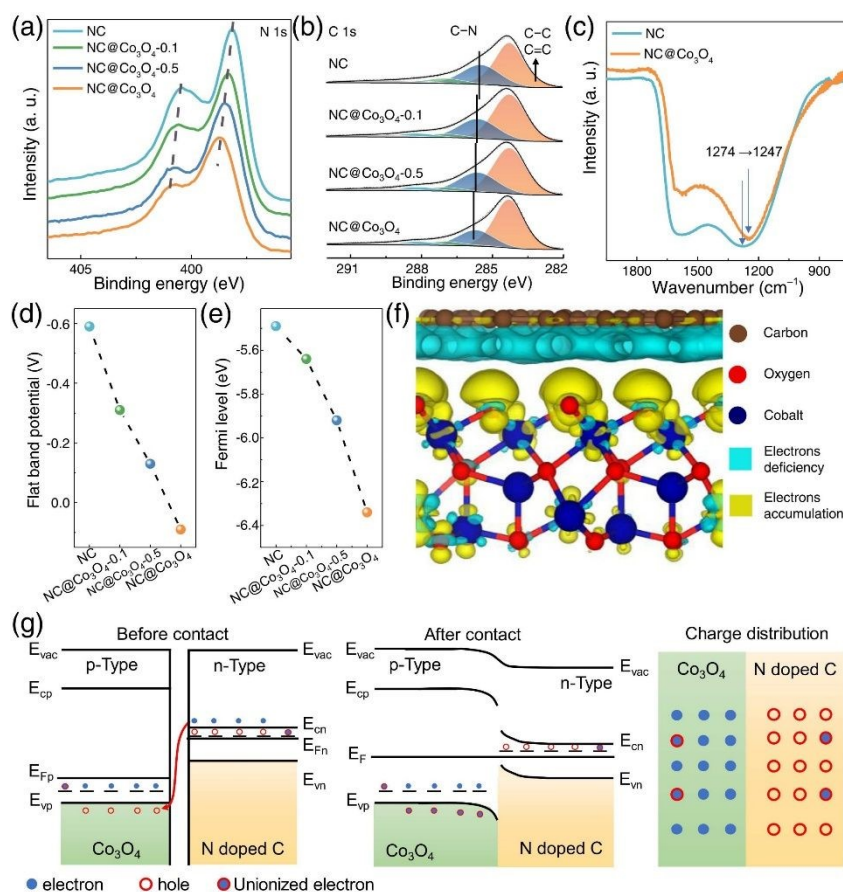
494 3.3. Hybrid Systems

495 3.3.1 Carbon-semiconductor heterostructures

496 Recently, several studies have been reported on the coupling of carbon-based materials with
497 metal oxides or nitrides to boost their 2e⁻ ORR activity.¹²²⁻¹²⁸ Generally, the structural
498 modulation of the carbon-metal oxide nanocomposites can rapidly release *OOH generated by
499 the metal oxides with high activity. For instance, Qu *et al.*¹²² reported the integration of CNTs
500 with g-C₃N₄ to improve both electrocatalytic activity and selectivity of CNT for H₂O₂
501 production by forming a π - π interaction at their interface. The optimal g-C₃N₄/CNT
502 nanocomposite catalyst exhibited almost unity (~97%) for H₂O₂ production at 0.50 V vs. RHE
503 with a 2 times current density of the pristine g-C₃N₄ or CNT. The enhanced activity can be
504 attributed to a synergistic effect, by which g-C₃N₄ provides active sites to activate O₂ while

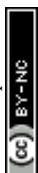


505 CNT offers channels to facilitate electron transfer. In addition, Guo *et al.*¹²⁹ designed and
 506 prepared a novel MnO_x @Carbon hybrid electrocatalyst by calcinating polymer-manganese-
 507 metal-organic framework (polyMn-MOF) as the precursor under N_2 atmosphere. DFT
 508 calculation revealed that the optimized MnO_x @Carbon sample exhibited optimized adsorption
 509 energy of $^*\text{OOH}$, with a high H_2O_2 selectivity of 96.5 % and large ORR current of 2.3 mA cm^{-2} .



510
 511 **Figure 12.** N-doped carbon and Co_3O_4 (NC@ Co_3O_4) p-n heterojunction nanocomposite for
 512 electrocatalytic H_2O_2 production. XPS spectra of (a) N 1s and (b) C 1s; (c) FTIR spectra of NC
 513 and NC@ Co_3O_4 ; (d) The flat band potential (E_{fb}) estimated from Mott-Schottky plots; (e) Fermi
 514 level measured by UPS; (f) Differential charge density of NC@ Co_3O_4 heterojunction; (g)
 515 Schematic illustration of energy band and electron transfer of NC@ Co_3O_4 p-n heterojunction.
 516 Reproduced with permission.¹²³ Copyright 2024, Elsevier.

517
 518 Recently, Xue *et al.*¹²³ reported a novel p-n heterojunction nanocomposite consisting of N-
 519 doped carbon and Co_3O_4 (NC@ Co_3O_4), for efficient electrocatalytic H_2O_2 production (**Figure**
 520 **12**). Increasing Co content results in a more positive flat band potential (E_{fb}), indicating a
 521 decrease of the Fermi level. In addition, the differential charge density calculation demonstrated

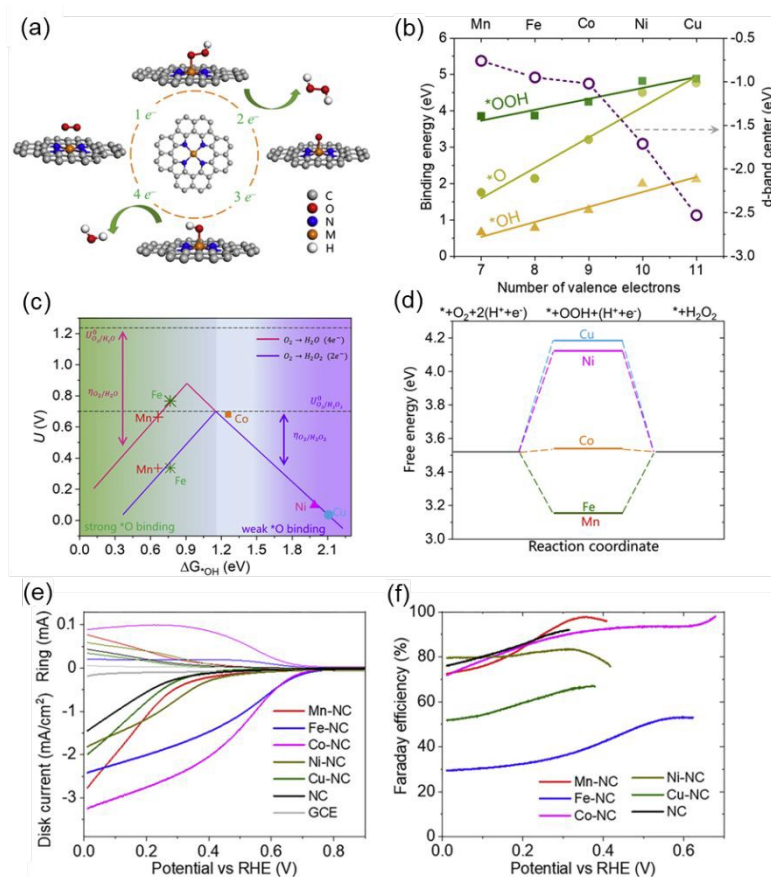


522 that the electrons of the NC are transferred to the Co_3O_4 and promotes the affinity of O atom of
523 H_2O_2 at the electron deficient carbon sites in NC, which facilitates the cleavage of O–O bonds.
524 Consequently, the $\bullet\text{OH}$ generation rate catalyzed by $\text{NC}@ \text{Co}_3\text{O}_4$ was 6.5 times of that by bare
525 NC. This work highlights the promising potential of constructing carbon/semiconductor
526 nanocomposite toward efficient H_2O_2 generation.

527 3.3.2 Atomic-site engineered carbon hybrids

528 Coordination of atomically dispersed transition metals single-atom catalysts (SACs) in a
529 carbon matrix have proven to be effective as ORR electrocatalysts, featuring a nearly 100%
530 utilization of metal atoms as active sites and excellent catalytic activity.^{130, 131} The electronic
531 structure of the SACs can be regulated benefiting from the strong interaction between metal
532 atoms and the substrate, and further modulates the adsorption energy of the catalyst for oxygen-
533 containing intermediates, which affects the 2e^- ORR selectivity.¹³²⁻¹³⁷ As such, different SACs
534 such as Co-SACs,^{136, 138-141} Zn-SACs,¹³³ Fe-SACs,¹⁴² Mn-SACs,¹⁴³ W-SACs,¹⁴⁴ Pt-SACs,^{145,}
535 ¹⁴⁶ Pd-SACs,^{83, 92} Pb-SACs,¹⁴⁷ Sn-SACs¹⁴⁸ and In-SACs¹⁴⁹ have displayed superior 2e^- ORR
536 performances for H_2O_2 production, showing large mass activity, low overpotential, and high
537 selectivity. In this part, we emphasis the most important achievements in this field by presenting
538 and discussing both experimental and theoretical investigations, especially the most recent
539 advancements on more complex systems using dual-single atom carbon catalysts or coupled
540 with other synergistic effects.

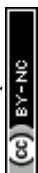




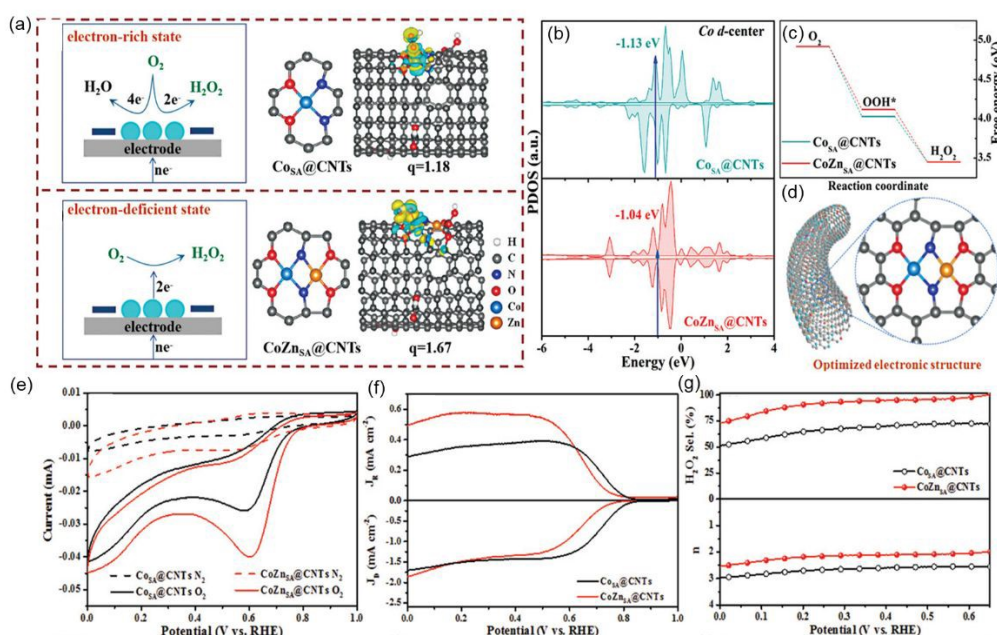
541

542 **Figure 13.** Transition metal SACs (M-SAC) (M = Mn, Fe, Co, Ni, and Cu) anchored in N-
 543 doped graphene electrocatalysts for producing H₂O₂. (a) Schematic of ORR; (b) Binding energy
 544 of *OOH, *O, and *OH on M-SAC and *d*-band center of different M atoms in M-SAC; (c)
 545 Volcano curves of ORR via the 2e⁻ and 4e⁻ pathway; (d) Free energy diagrams of 2e⁻ ORR on
 546 different M-SACs (0.7 V versus RHE); (e) LSV curves and (f) Faradic efficiency as a function
 547 of potential. Reproduced with permission.¹⁵⁰ Copyright 2020, Cell Press.

548
 549 Gao *et al.*¹⁵⁰ fabricated transition metal (Mn, Fe, Co, Ni, and Cu) SACs anchored N-doped
 550 graphene and systematically investigated their electrocatalytic performance for synthesizing
 551 H₂O₂ via ORR (**Figure 13a**). Theoretically simulations demonstrated that the Co-SAC
 552 possesses optimal *d*-band center, activity-volcano plot, and adsorption energy of the *OOH
 553 intermediate among all M- SAC samples (**Figure 13b-d**). As a result, the kinetic current for
 554 H₂O₂ production using Co SAC catalyst can reach up to ~1 mA cm⁻² (0.6 V vs. RHE in 0.1 M
 555 HClO₄) with faraday efficiency over 90% (**Figure 13e and f**), which even outperforms state-
 556 of-the-art noble-metal-based electrocatalysts in acidic media. Moreover, kinetic and in-situ X-



557 ray absorption analysis demonstrated that the N-coordinated single Co single-atom function as
 558 the active site for the reaction, which is rate-limited by the first electron transfer step.



559 **Figure 14.** (a) Illustration of the model and their differential partial charge densities with OOH*
 560 adsorption (side view); (b) PDOS of Co 3d orbital and (c) Gibbs free energy diagrams of two-
 561 electron ORR of Co_{SA}@CNTs and CoZn_{SA}@CNTs, respectively; (d) Schematic of optimized
 562 electronic structure; Electrochemical performance of CoZn_{SA}@CNTs and Co_{SA}@CNTs: (e) CV
 563 curves, (f) LSV curves based on RRDE, and (g) H₂O₂ selectivity and electron transfer number
 564 (*n*). Reproduced with permission.⁸⁵ Copyright 2024, Wiley-VCH.

565
 566
 567 Compared to well-studied SACs, dual-atom catalysts (DACs) have received considerable
 568 attention due to the synergistic interactions between two adjacent metal sites, leading to
 569 remarkably enhanced activity, selectivity, and stability. The dual sites facilitate multi-step
 570 reactions and improve binding energies for reactants and products. In addition, DACs are more
 571 resistant to aggregation and can offer tunable properties through metal pair selection, making
 572 them ideal for complex catalytic processes. Recent advancements in DAC design have
 573 demonstrated their superior electrocatalytic performance for H₂O₂ production through the 2e⁻
 574 ORR pathway.

575 In-N-C DACs was proposed by Du *et al.*¹⁵¹ as an effective 2e⁻ ORR catalyst for producing
 576 H₂O₂ in acid media. The DFT calculations indicate that the valance electron number and the *d*-



577 band center of Co 3d orbital can be modulated by OH-blocked In, which leads to moderate
578 adsorption of OOH intermediate on neighboring Co and favors 2e⁻ ORR kinetics of Co/In-N-C
579 DACs. As a result, a partial current density of 1.92 mA cm⁻² (0.65 V in the RRDE test) was
580 obtained, with a H₂O₂ production rate as high as 9680 mmol g⁻¹ h⁻¹ in a three-phase flow cell.
581 Very recently, Yang *et al.*⁸⁵ fabricated heteronuclear CoZn DACs confined in N,O-doped
582 hollow carbon nanotube reactors (CoZn_{SA}@CNTs) (**Figure 14**). The differential partial charge
583 density calculation demonstrated that the dual-atom centers in CoZn_{SA}@CNTs possess more
584 charges than that of Co_{SA}@CNTs (**Figure 14a**), indicating a rearrangement of the local charge
585 distribution to facilitate the adsorption of OOH* after introducing Zn. The decrease of the *d*-
586 band center in CoZn_{SA}@CNTs resulted in the appropriate adsorption of OOH* for
587 H₂O₂ generation (**Figure 14b**), while inhibited the breakage of O–O bond to produce H₂O,
588 ultimately facilitating the 2e⁻ ORR. In addition, CoZn_{SA}@CNTs model exhibited a more
589 favorable Δ*G*_{OOH*} than that of Co_{SA}@CNTs (**Figure 14c** and d). The well-designed
590 CoZn_{SA}@CNTs nanocomposite displayed outstanding electrocatalytic reactivity/selectivity for
591 generating H₂O₂ in the whole pH range (**Figure 14e-g**), with a higher 2e⁻ ORR selectivity for
592 H₂O₂ production than Co_{SA}@CNTs and Zn_{SA}@CNTs. In a H-type cell, CoZn_{SA}@CNTs/carbon
593 fiber felt reached nearly 100% H₂O₂ selectivity in a range of 0.2–0.65 V (vs. RHE) with a yield
594 rate of 1500 mmol g⁻¹ h⁻¹, surpassing most of the reported SACs. These studies highlight the
595 great advantages of using DACs/carbon for highly efficient and selective H₂O₂ production.

596 3.4. Synergistic integration of multiple effects

597 The integrating of different effects, such as morphological control, engineering, and single-
598 atom site design, creates a synergistic interplay that elevates catalytic performance beyond the
599 simple sum of individual components. The coupling effect simultaneously enhances mass
600 transport efficiency, electronic structure modulation, and atomic-level active site utilization,
601 collectively optimizing the reaction pathways and maximizing overall catalytic efficiency.



602 Below, we discuss key coupling strategies to date, providing insights to guide future
603 advancements in rational design of carbon-based electrocatalysts.

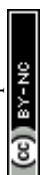
604 3.4.1 Coupling defect/surface group with microstructure

605 Carbon materials with diverse porous structures have been reported, with simultaneously
606 introduction of surface functional groups. For instance, Albashir *et al.*¹⁵² fabricated mesoporous
607 material (Meso-PC) functionalized with ketonic carbonyl ($-\text{C}=\text{O}$) group, which exhibits
608 outstanding 2e^- ORR selectivity ($\sim 100\%$) at the potential of $0.4 \text{ V}_{\text{RHE}}$. This can be attributed to
609 its precisely tailored pore structure, which facilitates the mass transfer of reactants and products.
610 Furthermore, studies suggest that the $-\text{C}=\text{O}$ group serve as the primary active site for 2e^- ORR,
611 while a moderate surface concentration of oxygen functionalities is crucial to enhancing
612 electrochemical H_2O_2 synthesis activity.

613 In addition, Jing *et al.*⁹⁰ demonstrated that N,O co-doped carbon nanosheets (N,O-CNS) with
614 a hierarchical micro/mesoporous structure can create an oxygen-rich, locally alkaline-like
615 microenvironment, significantly promoting the 2e^- ORR pathway in a neutral medium. Their
616 study revealed that the hierarchical architecture not only elevates the local pH near the active
617 sites but also facilitates the formation of intermediates ($^*\text{O}_2$ and $^*\text{OOH}$), thereby enhancing
618 H_2O_2 selectivity and yield. Remarkably, the optimized N,O-CNS_{0.5} catalyst achieved an
619 exceptional H_2O_2 production rate of $6705 \text{ mmol g}^{-1} \text{ h}^{-1}$ in a flow cell, setting a new benchmark
620 for neutral-media electrocatalysis. This work highlights the critical role of synergistic
621 microenvironment engineering, which combines pore structure control, heteroatom doping, and
622 local pH modulation, in designing high-performance electrocatalysts for sustainable H_2O_2
623 synthesis.

624 3.4.2 Coupling atomic active sites with microstructures

625 Coupling SACs with other tailoring strategies such as microstructure modulation of carbon
626 materials can lead to novel synergistic effects to further boost the electrocatalytic performance.
627 As a notable example, atomically dispersed Co/Mo sites anchored on mesoporous carbon



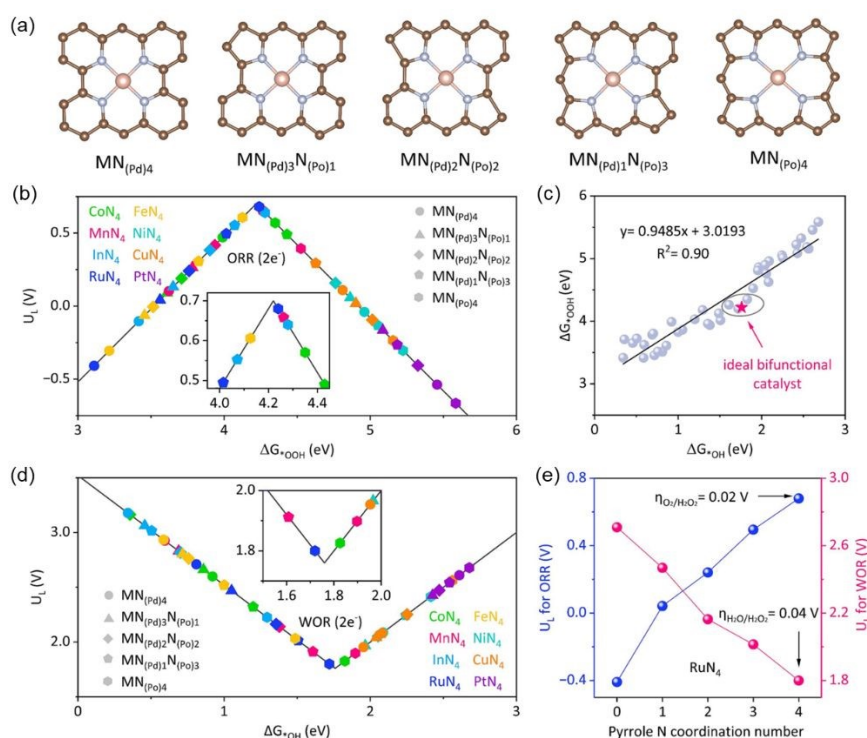
628 hollow spheres (Co/Mo-MCHS) via a template-engaged strategy for highly selective ORR to
629 H_2O_2 in acid.¹⁵³ Benefitting from the electron-donating effect of Mo atoms, an enriched electron
630 density around the Co center for Co/Mo-MCHS is observed, resulting in optimal adsorption of
631 the key $^*\text{OOH}$ intermediates to approach the apex of 2e^- ORR volcano plot. Moreover, the
632 introduction of Mo species simultaneously suppresses the electroreduction of as-obtained
633 H_2O_2 on Co sites. Owing to the integration of mesoporous hollow merits and electron-donating
634 effect, the Co/Mo-MCHS electrocatalyst displays efficient 2e^- ORR pathway with a noticeable
635 ring current response and high H_2O_2 selectivity of 90–95% over the wide potential range in
636 acid. After long-term operation over 15 h, 90% of the initial H_2O_2 selectivity could be retained.
637 For large-scale electrolysis, a remarkable H_2O_2 yield of 2102 mg for 150 h is obtained,
638 suggesting great potential for practical applications. This study provides valuable guidance for
639 the rational design of more complex SACs/carbon catalysts by combing different effects in the
640 future.

641 3.4.3 Coupling electronic defects with atomic active sites

642 Liu *et al.*¹⁵⁴ systematically investigated a series of metals catalysts anchored on nitrogen-
643 doped carbon (M-NC), including representative transition metals (Mn, Fe, Co, and Ni), *4d*
644 transition metal (Ru), *5d* transition metal (Pt), and non-transition metal (In), to assess their
645 activity for synthesizing H_2O_2 (**Figure 15**). Four types of M-NC catalysts with different
646 pyridine and pyrrole N atoms ratios were constructed (**Figure 15a**). The 2e^- ORR activity
647 volcano plot for total 40 SAC configurations were examined through DFT calculations (**Figure**
648 **15b**). The coordination environment can tune the $\Delta G_{^*\text{OOH}}$ position in M-NCs significantly, with
649 the highest value occurred at $\text{MN}_{(\text{P}_0)_4}$ type catalysts for each metal. Meanwhile, the
650 corresponding $\Delta G_{^*\text{OH}}$ and 2e^- WOR volcano curve were also calculated (**Figure 15c**),
651 demonstrating that pyrrolic-N affect the adsorption of OH, and the free energy shift is almost
652 consistent with $^*\text{OOH}$. Considering the ORR and WOR reaction pathway together, the $\text{CoN}_{(\text{P}_0)_4}$,
653 $\text{MnN}_{(\text{Pd})1}\text{N}_{(\text{P}_0)_3}$ and $\text{RuN}_{(\text{P}_0)_4}$ show promising prospects as bifunctional SAC for H_2O_2 generation.



654 Considering the fitting curve of ΔG_{*OH}^* and ΔG_{*OOH}^* (**Figure 15d**) and all key factors including
 655 overpotential, reaction kinetics, transition state energy, and thermodynamic stability, RuN_{(Po)₄}
 656 SAC are the most promising candidate for efficient H₂O₂ generation, and the pyrrole N
 657 coordination can modulate the 2e⁻ ORR/WOR kinetics (**Figure 15e**). This study provides deep
 658 theoretical insights into regulating coordination structure for the rational design of high-
 659 efficient and stable bifunctional SACs/carbon catalysts for H₂O₂ production.



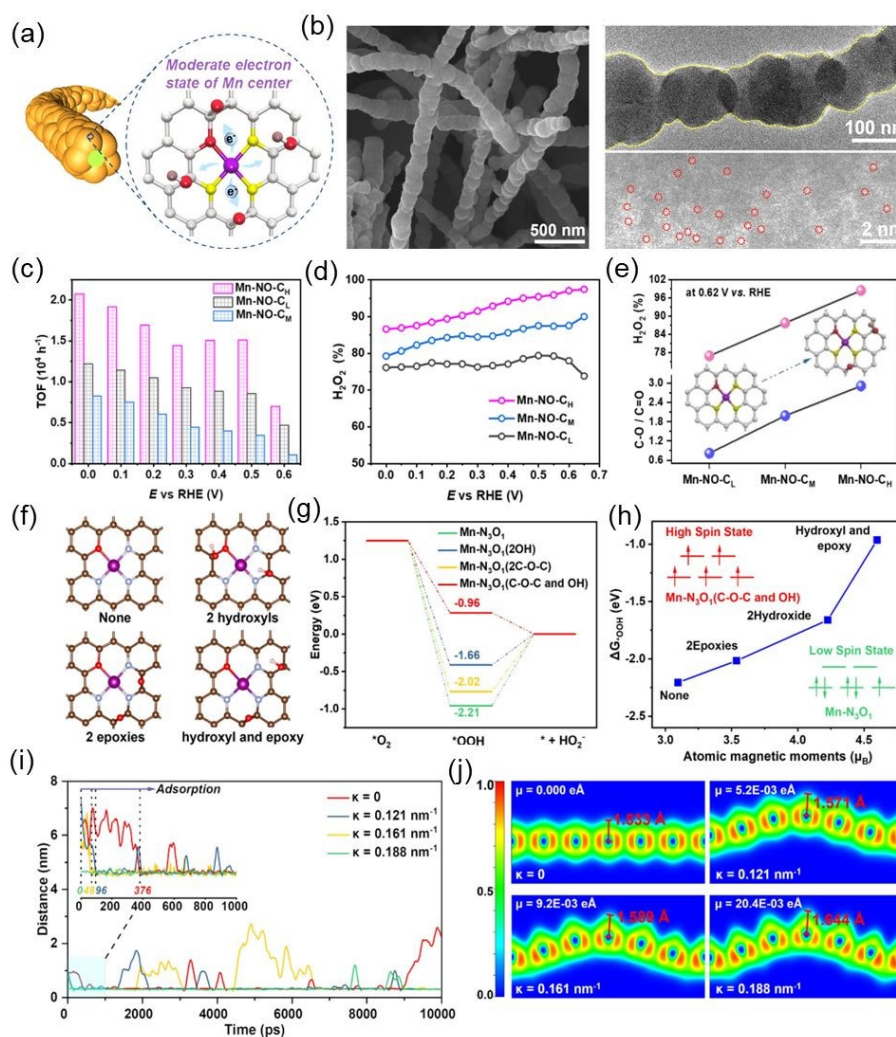
660
 661 **Figure 15.** DFT calculation on various metal SAC catalysts anchored on nitrogen-doped carbon
 662 (M-NC) for H₂O₂ production via 2e⁻ ORR and 2e⁻ WOR. (a) Optimized MN₄ structure with
 663 different pyrrole N coordination numbers; Activity volcano relation for (b) 2e⁻ ORR and (c)
 664 2e⁻ WOR between intermediates formation energy and limiting potential; (d) Scaling plots
 665 between ΔG_{*OH}^* and ΔG_{*OOH}^* ; (e) Relationship between pyrrole N coordination numbers and
 666 limiting potential for 2e⁻ ORR and 2e⁻ WOR of all Ru-NC catalysts. Reproduced with
 667 permission.¹⁵⁴ Copyright 2023, Elsevier.
 668

669 3.4.4 Multiple synergistic effects

670 The integration of multiple effects creates a powerful synergistic platform that overcomes
 671 the limitations of binary coupling, which can further maximize the overall catalytic efficiency.
 672 A representative example involves the rational design of highly porous open carbon nanocages

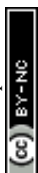


673 with embedded Co nanoparticles (NPs) fabricated through a template-assisted method.¹⁵⁵ The
 674 optimized P-Co@C-700 catalyst exhibits several intergrating effects, including highest
 675 percentage of –C–O–C group and defects, embedding Co NPs, and mesoporous structure,
 676 resulting in a high selectivity up to 94% toward H₂O₂ production in 0.1 m HClO₄. Benefiting
 677 from the synergistically modulated electronic and pore structure, the optimized open carbon
 678 nanocages exhibit outstanding activity, selectivity, and stability for 2e⁻ H₂O₂ production in
 679 acidic condition.



680

681 **Figure 16.** (a) The schematic of heterogeneous catalyst composed of boundary-rich carbons
 682 supported active Mn(II) centers (Mn–NO–C_H) with selective oxygen functional groups. (b)
 683 SEM, TEM and HAADF-STEM images of Mn–NO–C_H. (c) TOFs, (d) H₂O₂ selectivity, and
 684 (e) correlation between H₂O₂ selectivity (0.62 V vs. RHE) and the proportion of oxygen species.
 685 (f) The DFT models for Mn–N₃O₁. (g) The calculated free energy at 0 V vs. RHE for 2e⁻ORR
 686 pathway. (h) The correlation between magnetic moment and the free energy for Mn–N₃O₁ after
 687 *OOH adsorption. (i) MD simulation for the minimum distance between O₂ molecules and C



688 atoms. (j) Electronic Localization Function mapping images with different curvatures
689 Reproduced with permission.¹⁴³ Copyright 2024, Wiley-VCH.

690
691 Moreover, as a notable example, Dong *et al.*¹⁴³ developed a novel Mn SACs-coordinated
692 boundary-rich porous carbon-based electrocatalysts (**Figure 16a** and **b**), in which the secondary
693 coordinated epoxide, hydroxyl groups surrounding the Mn–N₃–O centers, and the boundary-
694 rich morphology together lead to the predominant selectivity and efficiency for H₂O₂
695 production through the 2e⁻ ORR pathway. The catalysts exhibited nearly 100 % Faradaic
696 efficiency and with a reaction rate up to 15100 mmol g_{cat}⁻¹ h⁻¹ (0.1 V vs. RHE), achieving the
697 record activity for Mn-based electrocatalyst for electrosynthesis of H₂O₂ (**Figure 16c-e**).
698 Mechanistic investigations indicate that the epoxide and hydroxyl groups surrounding the
699 Mn(II) centers promote spin state and tailor the adsorption of *OOH intermediate, and
700 multiscale simulations reveal that the high-curvature boundaries can promote adsorption and
701 local enrichment of O₂ (**Figure 16f-j**). Such synergy highlights the importance of holistic
702 material design, where defects, doping, and atomic-scale engineering work in concert to achieve
703 greatly improved performance.

704 To comprehensively evaluate the advantages and limitations of carbon-based electrocatalysts
705 for H₂O₂ production, it is essential to compare them with non-carbon-based catalyst systems,
706 such as metal oxides and noble-metal catalysts. **Table 1** summarizes the critical metrics (onset
707 potential, H₂O₂ selectivity, production rate, and stability) across different representative catalyst
708 types. Although Pt/Pd-based noble metal-based catalysts are recognized as efficient catalysts
709 with small overpotential and high selectivity for 2e⁻ ORR, their industrial-scale application is
710 greatly limited by scarcity, high cost, and susceptibility to poisoning.^{24, 41, 156, 157} Metal oxide
711 electrocatalysts demonstrate excellent stability, while achieving high selectivity remain
712 challenging.¹⁵⁸ Although some recently reported metal oxides such as *h*-SnO₂ demonstrate
713 superb electrocatalytic activity,¹⁵⁹ but still suffer from poor stability in electrolyte. Furthermore,
714 synthesizing high active metal oxide catalysts often requires complex procedures and precise



715 control over their structure and composition. It is also worth noting that the emerging
716 MOF/COF materials show high production activity but poor stability.

717 We have summarized the most representative carbon-based materials for electrocatalytic
718 H₂O₂ production reported in the past few years (**Table 2**), systematically classified by materials
719 design categories: microstructure tailoring, defect engineering (including intrinsic and
720 heteroatom doping), surface functional group modulation, and single-atomic site configurations.
721 In comparison, carbon-based electrocatalysts offer distinct advantages, including low-cost and
722 widely availability, making them highly attractive for large-scale applications. Up till now, the
723 performance of carbon-based electrocatalyst is comparable or even outperforming many noble
724 metal-based systems, maintaining cost and environmental benefits. Carbon-supported single-
725 atom catalysts (SACs) achieve high production rates of ~500–30,000 mmol·g⁻¹·h⁻¹. However,
726 the activity and stability of carbon catalysts in neutral or weakly acidic environments still needs
727 to be further improved, as well as mitigating degradation during long-term electrochemical
728 operation.

729 The stability of carbon-based electrocatalysts for H₂O₂ production varies significantly across
730 different categories, with durations ranging from a few hours to ~250 h. Microstructure-
731 modulated catalysts like graphitic ordered mesoporous carbon (O-GOMC) exhibit high stability
732 (168 h) due to robust porous frameworks, while defect-engineered materials such as B-doped
733 carbon demonstrate durability (100 h) under high current densities. Surface modifications,
734 including polymer coatings or metal complexes, demonstrated relatively low stability as
735 evidenced by CoPc-carbon (24 h). Although single-atom catalysts generally exhibit very short
736 lifetime (~10 h), recently reported synergistic systems such as Pb SAs/OSC (100 h) and N,S-rich
737 carbon nanotubes (200 h) are highly promising. Challenges still remain in standardizing testing
738 protocols and achieving long-term stability for industrial applications. Future research should
739 focus on elucidating degradation mechanisms and optimizing catalyst designs for extended
740 operational lifetimes.



741

View Article Online
DOI: 10.1039/D5MH00221D742 **Table 1.** Comparison of performance with representative non-carbon-based systems.

Type	Catalysts	Selectivity (%)	H ₂ O ₂ production rate	Electrolyte	Stability	Ref.
Noble metals	PtP ₂	98.5	2.26 mmol·h ⁻¹ ·cm ⁻²	0.1 M HClO ₄	120 h	160
	Pt-Hg/C	>90	/	0.1 M HClO ₄	8000 cycles	24
	Pt ₁ -CuS _x	92–96	546 mmol·g ⁻¹ ·h ⁻¹	0.1 M HClO ₄	10 h	161
Oxides	Pt ₁ /CoSe ₂	/	110.02 mmol·g ⁻¹ ·h ⁻¹	0.1 M HClO ₄	60 h	162
	h-SnO ₂	99.9	3885.26 mmol·g ⁻¹ ·h ⁻¹	0.1 M Na ₂ SO ₄	20 h	159
	α-Fe ₂ O ₃	80.5	546.8 mmol·g ⁻¹ ·h ⁻¹	0.1 M KOH	48 h	158
Carbon-based	Single atoms-carbon	96.5	12510 mmol·g ⁻¹ ·h ⁻¹	0.1 M KOH	12 h	163
	N/S-CNTs	90.0	30370 mmol·g ⁻¹ ·h ⁻¹	1.0 M KOH	200 h	164
Other systems	B-doped carbon MOF	88.7	24300 mmol·g ⁻¹ ·h ⁻¹	0.1 M KOH	100 h	165
	nanosheets	99	6500 mmol	0.1 M KOH	11 h	166
	Boron nanosheets	~90	25100 mmol g ⁻¹ h ⁻¹	1.0 M Na ₂ SO ₄	140 h	167

743



744 **Table 2.** Summary of representative carbon-based materials for electrocatalytic H₂O₂ production.

Type	Catalysts	Electrolyte	Onset potential (V vs. RHE)	H ₂ O ₂ selectivity (%)	Production rate	Voltage (V vs. RHE)	Faradaic efficiency (%)	Tafel slope (mV·dec ⁻¹)	Stability	Ref.
Microstructure modulation	Carbon mesoporous nanoreactors (MHCS)	0.1 M KOH	0.6	85	3.36 mmol·L ⁻¹ ·h ⁻¹	0.5	97	73	12 h	168
	Graphitic ordered mesoporous carbon (O-GOMC)	0.1 M KOH	0.75	~92	63.33 mg·L ⁻¹ ·h ⁻¹	0.6	99.2	42	168 h	169
	O-GOMC	0.1 M KOH	0.73	93±1	24 mmol·L ⁻¹	/	99	59	16 h (3 mA)	170
	Honeycomb carbon nanofibers (HCNFs)	0.1 M KOH	0.87	97.3	6.37 mmol·L ⁻¹ ·h ⁻¹ (0.05 mg)	0.5	/	75.6	12 h	171
	Porous carbon (PCC ₉₀₀)	0.1 M KOH	0.83	95	1696.8 mmol·g ⁻¹ ·h ⁻¹	/	90	38	10000 times	172
	Hollow mesoporous carbon sphere (HMCSs)	0.1 M KOH	0.82	95	/	0.53	87	/	10 h	173
	Mesoporous carbon-nanofibers (MCNF)	0.1 M KOH	0.68	>90	/	0.4	>85	43	12 h	174
	Holey graphene	0.1 M KOH	0.56	95	2360 mmol·g ⁻¹ ·h ⁻¹	0.1	97	/	12 h	175
	Oxidized carbon nanotubes	0.1 M KOH	0.795	>90	/	4	>85	38	96 h	176
	Oxygen-doped carbon quantum dots	0.1 M KOH	/	96.2	338.7 mmol·g ⁻¹ ·h ⁻¹	-1.33	92	66.95	120 h	177
Defect engineering	Oxygen modified defective graphene	0.1 M KOH	0.9	98.38	41.45 mg·cm ⁻² ·h ⁻¹	0.5	95	/	10	178
	Doped carbon nanohorns	0.1 M KOH	0.85	>80	740 mmol·g ⁻¹ ·h ⁻¹	0.65	50-100	49	12 h	179
	B-doped carbon	0.1 M KOH	0.780	88.7	24300 mmol·g ⁻¹ ·h ⁻¹	/	82	51	100 h (100 mA·cm ⁻²)	165
	B-doped nanocarbon	0.1 M KOH	0.78	95	247 mg·L ⁻¹ ·h ⁻¹	0.5	100	/	10 h	180



	B-doped carbon	0.1M KOH	0.773	95	7.36 mmol·cm ⁻² ·h ⁻¹	/	90	78	30 h (200 mA·cm ⁻²)	181
	N-doped carbon spheres	0.1 M KOH	0.7	91.9	618.5 mmol·g ⁻¹ ·h ⁻¹	0.4	85.1	/	10 h	182
	N-doped graphene	0.1 M KOH	0.764	>82	224.8 mmol·g ⁻¹ ·h ⁻¹	0.3	>43.6	/	4 h	183
	N-doped carbon	0.1 M HClO ₄	0.6	80-98	2923 mg·L ⁻¹ ·h ⁻¹	0.3	100	136.6	10 h	184
	N-doped carbon	0.5 M NaCl	0.61	95	631.2 mmol·g ⁻¹ ·h ⁻¹	0.51	79.8	79	10 h	185
	N,O co-doped carbon nanosheets	0.1 M K ₂ SO ₄	0.65	>90	6705 mmol·g ⁻¹ ·h ⁻¹	0.2	91	52	24 h	186
	Polydopamine modified carbon (CB-PDA-A)	0.1 M KOH	0.8	80	1800 mmol·g ⁻¹ ·h ⁻¹	1.5	95	70	250 h	61
	CoPc-carbon	0.1 M KOH	0.7 V	99%	10400 mmol·g ⁻¹ ·h ⁻¹	0.2	93	54	24 h	187
Surface modification	Polymerization of acrylonitrile (PNAC-F)	0.1 M KOH	0.78	93	816 mmol·g ⁻¹ ·h ⁻¹	0.78	/	/	40 h	188
	Carbon black	0.1 M KOH	0.75	96	/	0.33	/	60	10 h	189
	Activated coke@carbon cloth	0.1 M Na ₂ SO ₄	/	100	30.41 mg·h ⁻¹ ·cm ⁻²	/	80	104.1	10 h	190
	N-B-OH-Graphene quantum dots	0.1 M KOH	0.7	90	709 mmol·g ⁻¹ ·h ⁻¹	0.2	81	/	12 h	191
	Pb-carbon dot (Pb SAs/OSC)	0.10 M KOH	0.65	>90	6.9 mmol·cm ⁻¹ ·h ⁻¹	/	92.7	49	100 h (50 mA·cm ⁻²)	192
Single-atom/carbon hybrids	Single atoms cellulose-carbon (FeSAs/ACs-BCC)	0.1 M KOH	0.78	96.5	12510 mmol·g ⁻¹ ·h ⁻¹	0.4	89.4	73	12 h	163
	In single atoms on carbon (In SAs/NSBC)	0.1 M KOH	0.66	95	6490 mmol·g ⁻¹ ·h ⁻¹	0.3	75	30.3	12 h	193
	Pt single atoms-g-C ₃ N ₄ (Pt _{0.21} /CN)	0.1 M KOH	0.81	98	767 mmol·g ⁻¹ ·h ⁻¹	0.6	96	/	10 h	194



	Metal-nitrogen-carbon	0.1 M HClO ₄	0.75	>70	688 mmol·g ⁻¹ ·h ⁻¹	0.3	93	113	12 h	195
	CoZn-N/O-carbon nanotube (CoZn _{SA} @CNTs)	0.1 M KOH	/	90-100	4770 mmol·g ⁻¹ ·h ⁻¹	0.2	95	76.3	5 h	196
	Co-O ₄ porous graphene-like carbon (Co-O ₄ @PC)	0.1 M KOH	0.73	98.8	250 mmol·g ⁻¹ ·h ⁻¹	0.5	/	72	10 h	197
	Co-N ₄ C-O-C epoxide groups	0.1 M KOH	0.801	91.3	6912 mmol·g ⁻¹ ·h ⁻¹	0.09	/	51.3	10 h	198
	Atomic metal-nitrogen-carbon (F/Co-N-G SAC)	0.1 M KOH	0.810	94.2	12100 mmol·g ⁻¹ ·h ⁻¹	0.1	70	45.2	10 h	199
	S,N-coordinated Ni SAC (Ni-N ₃ S)	0.1 M KOH	0.80	90.0	17500 mmol·g ⁻¹ ·h ⁻¹	0.2	85	/	12 h	200
	Bipyridyl N-carbonyl (Pd-N ₂ O ₂ -C)	0.1 M KOH	0.82	95	1.5×10 ⁷ mmol·g ⁻¹ ·h ⁻¹	0.4	/	/	10 h	201
Synergistic effects	Pd atoms on nitrogen-doped carbon (Pd-NC)	0.1 M KOH	0.8	95	30 mmol·g ⁻¹ ·h ⁻¹	0.5	/	56	8 h	202
	Carbon-based single atom (Zn-N ₂ O ₂ -S SAC)	0.1 M KOH	/	96	6924 mmol·g ⁻¹ ·h ⁻¹	/	93.1	62	65 h (80 mA·cm ⁻²)	203
	Co SACs-carbon nanofiber (Co@EO-ACNF)	0.1 M KOH	/	85.21	15750 mmol·g ⁻¹ ·h ⁻¹	0.6	84.5	/	48 h	204
	W SAC on O,N-doped carbon (W ₁ /NO-C)	0.1 M KOH	0.815	>90	1230 mmol·g ⁻¹ ·h ⁻¹	0.6	95	115	20 h	205
	Pd-oxidized carbon nanotubes	0.1 M HClO ₄	0.7	95	1700 mmol·g ⁻¹ ·h ⁻¹	0.1	93	/	8 h	74
	Defective carbon (Mo-CDC-ns)	0.1 M KOH	0.75	90	455 mmol·g ⁻¹ ·h ⁻¹	0.55	85.1	95-99	12 h	206
	Co@carbon nanocages	0.1 M HClO ₄	0.60	94	57 mmol·g ⁻¹ ·h ⁻¹	0.31	/	107.9	10 h	207

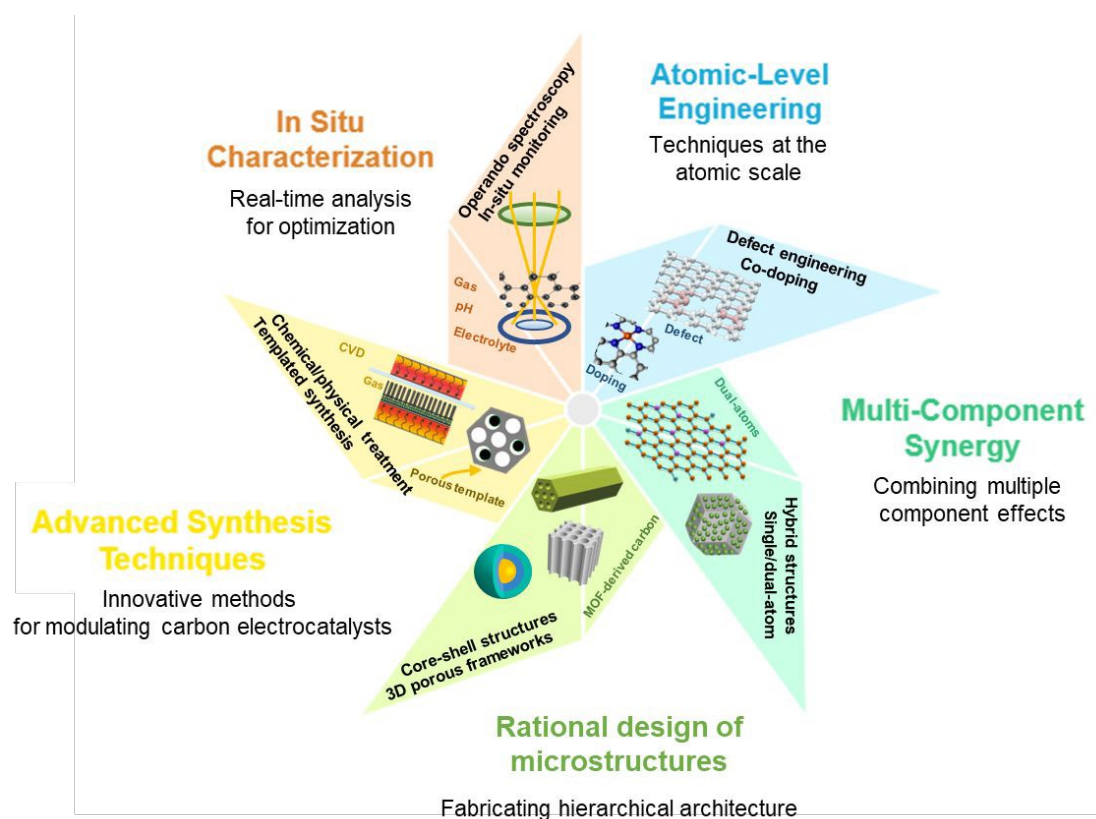


745

Ni SAC-carboxyl-multiwall carbon nanotubes (N ₄ Ni ₁ O ₂ /OCNTs)	1 M KOH	0.68	/	5.7 mmol·cm ⁻² ·h ⁻¹	/	96.1	107	24 h (200 mA·cm ⁻²)	208
Oxygen-vacancy-graphene armor (B/N-HCNS@V-G)	1 M KOH	0.79	91	55 ppm	0.5	94	63	24 h	209
Carbon nanotubes with N,S-rich tips (N, S-TCNTs)	1 M KOH	0.78	90.0	30370 mmol·g ⁻¹ ·h ⁻¹	/	>90	55.5	200 h (100 mA)	164

746 4. Conclusions and perspective

747 The electrochemical production of H₂O₂ using carbon-based nanomaterials has gained
 748 considerable research attention as an environmentally friendly, low-cost and efficient method.
 749 Substantial efforts have been made both experimentally and theoretically on 2e⁻ ORR
 750 electrocatalysis, with a focus on the structural-property relation and design of efficient carbon-
 751 based electrocatalysts. In this review, we summarized the key advancements in the materials
 752 design strategy. These studies demonstrate that modifying the local atomic structure of carbon
 753 materials, incorporating functional surface groups, doping with foreign atoms, tailoring
 754 microstructure, and introducing semiconductor or single-atomic sites can enhance not only the
 755 activity and selectivity for H₂O₂ production but also the long-term stability of these catalysts.
 756 These developments open the door to more efficient and scalable electrocatalytic processes for
 757 green H₂O₂ production.

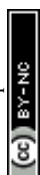


758
 759 **Figure 17.** Schematic of perspective strategies for rational design of carbon catalysts (atomic
 760 level engineering, multiple-synergistic effects), advanced synthesis method, and in-situ
 761 characterization techniques.



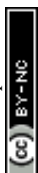
762
763 Despite the considerable progress achieved, challenges remain for the industrial-scale
764 implementation of electrocatalytic H₂O₂ production using carbon-based materials, including
765 improving electrocatalytic activity, ensuring long-term stability, and developing practical
766 designs for carbon-based electrodes and reactors. Therefore, advancing carbon electrocatalyst
767 design to achieve high activity and selectivity has become a primary focus in this field.
768 Furthermore, innovation in catalyst preparation, optimization of the activity and selectivity, as
769 well as deeper understanding of mechanisms are crucial to further advancing H₂O₂ production
770 in an environmentally benign manner more effectively. To date, carbon-based electrocatalysts
771 has demonstrated remarkable progress, driven by advances in engineering strategies that have
772 significantly improved catalyst performance over traditional methods. In the following section,
773 we will summarize and discuss the challenges and future perspectives in this research area
774 (**Figure 17**), including the rational design of carbon catalysts (e.g., atomic level engineering,
775 multiple-synergistic effects), advanced synthesis method, in-situ characterization techniques,
776 and system-level device design considerations for industrial applications.

777 The catalytic activity of carbon-based materials still has significant potential for further
778 improvement. Multiple synergistic modification strategies can be employed, including defect
779 engineering (e.g., creating vacancies and edge sites to promote O₂ adsorption), chemical doping
780 (e.g., introducing N, B, or S heteroatoms to tune electronic structure), facet control (e.g.,
781 exposing specific crystal planes with optimal *OOH intermediate binding energy), surface
782 active site design (e.g., atomically dispersed metal-N₄ moieties), interface engineering (e.g.,
783 constructing hybrid metal oxide/carbon junctions to facilitate charge transfer), and
784 microstructural modulation (e.g., developing hierarchically porous architectures to improve
785 mass transport). Although existing strategies have made notable progress in the electrosynthesis
786 of H₂O₂, the precise control of defects and single-atomic sites in carbon materials requires
787 further investigation to optimize the balance between the intrinsic activity and selectivity of



788 active sites. To precisely engineer defects in carbon-based materials, several methodologies can
789 be utilized: (1) plasma irradiation (Ar, N₂, or O₂) for controlled introduction of vacancies and
790 edge defects; (2) mechanical exfoliation techniques such as ball-milling or ultrasonication to
791 create strain-induced defects; and (3) pyrolysis of metal-organic frameworks (MOFs) to derive
792 defect-rich carbon matrices with atomic-level precision. Moreover, to promote mass transfer
793 process, tailoring the morphology of the catalysts with well-designed 3D hierarchically porous
794 architectures can significantly increase the availability of active sites and accelerate the
795 diffusion of reactants. The pore sizes and distribution need to be carefully designed to balance
796 the retention time and selective H₂O₂ production, reactant diffusion, resistance and reaction
797 kinetics. Specific methods include the use of sacrificial templates (e.g., mesoporous silica,
798 PMMA spheres, and amphiphilic block copolymers), combine with resins (e.g., resorcinol-
799 formaldehyde) for ordered mesopores, or add macroporogen (e.g., emulsion droplets) for triple
800 porosity. In addition, it is crucial to introduce surface functional groups (e.g., -COOH or -OH)
801 to tune hydrophilicity for improving electrolyte accessibility and modifying intermediate
802 binding strength through dipole interactions. For single-atom carbon catalysts, the
803 uncontrollable selectivity and poor stability remain critical challenges. The implement of
804 atomic layer deposition (ALD) for depositing protective layer (e.g., Al₂O₃ or TiO₂ sub-
805 nanolayers) can be used to enhance the stability while allowing reactant access; creating
806 proximal dual-atom sites is effective to promote the selectivity by modulating the O-O bond
807 cleavage. Critically, the synergistic integration of these strategies represents a pivotal research
808 direction for achieving sustained high selectivity in the 2e⁻ oxygen reduction pathway. Beyond
809 catalyst design, the role of the electrolyte in H₂O₂ production also deserves attention, as it can
810 influence the stability of the key intermediate *OOH, thereby regulating the overall efficiency
811 of H₂O₂ formation. And the ORR activity through the 2e⁻ pathway remains limited for many
812 carbon-based materials in neutral or weakly acidic environments.

View Article Online
DOI: 10.1039/D5MH00221D



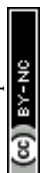
813 Beyond materials design, elucidating the fundamental electrocatalytic mechanisms remains
814 a critical research priority. At this moment, the reaction mechanisms of carbon-based
815 electrocatalysts remain insufficiently understood. It is worth noting that the active sites in
816 carbon catalysts typically undergo dynamic evolution during electrochemical reactions,
817 necessitating the study of these changes to fully explore the reaction mechanisms. To this end,
818 a comprehensive understanding of reaction pathways, active site dynamics under operational
819 conditions, and interfacial phenomena is essential for rationally guiding catalyst optimization.
820 Therefore, various in-situ/operando characterization techniques are needed to directly probe
821 reactive intermediates, active sites, and their interactions during electrochemical H₂O₂
822 generation process. For instance, in-situ XRD and X-ray absorption spectroscopy (XAS) can
823 be employed to analyze the local coordination environment, electronic structure, and oxidation
824 state of catalysts in real time. In addition, in-situ Raman and FTIR spectroscopy are valuable
825 for real-time detection of reaction intermediates during electrocatalysis reactions. Further
826 improvement in spatial and temporal resolution for in situ detection of dynamic electrocatalytic
827 processes is also desirable. To gain deeper insights into electrocatalytic mechanisms, advanced
828 theoretical calculations are needed to quantitatively correlate the energetics of intermediates
829 with reaction kinetics. With ongoing advances in computational power, algorithms, and big data
830 from both experiments and simulations, machine learning could play a transformative role in
831 predicting structure-performance relationships at previously unattainable scales. At present, the
832 2e⁻ WOR has received less attention and is in its early stages of development compared to the
833 2e⁻ ORR. Thus, the development of novel computational approaches to screen and guide the
834 design of advanced carbon-based 2e⁻ WOR electrocatalysts is essential. A fundamental
835 mechanistic understanding will elucidate the critical interplay between: (1) reaction
836 intermediate energetics, (2) surface-dependent selectivity determinants (e.g., *OOH binding
837 strength, local coordination environments), and (3) electrochemical microenvironment effects

View Article Online
DOI: 10.1039/D5MH00221D



838 (pH, potential, double-layer structure), ultimately enabling rational design of efficient H₂O₂ production systems.
839

840 While catalyst design has advanced significantly, it is worth noting that the development
841 of electrochemical reactors has lagged behind catalyst design in the past decade. Therefore,
842 system-level optimization is essential for practical implementation of carbon-based
843 electrocatalysts. Particular emphasis should be placed on the design of the overall
844 electrochemical system and the operational reliability of the industrial-grade device for
845 practical applications. Key considerations include O₂ mass transfer, device design, electrolyte
846 selection, ion exchange membranes, and reactor configurations. First, the mass transfer and
847 diffusion of reactant species within the interface microenvironment of the carbon electrode
848 needs further investigation.²¹⁰ Specific optimization strategies involve gas diffusion electrodes
849 with hierarchical porosity (macro/meso/micro pores) to balance O₂ transport and flow-through
850 membrane reactors with rotational cathodes. The use of porous solid electrolyte (PSE) reactor
851 for producing high-concentration and high-purity H₂O₂ may meet the high stability
852 requirement.²¹¹ In addition, optimizing local reaction environments—such as water
853 permeation/wetting, hydrophobicity/hydrophilicity, and reactant concentration—can enhance
854 the performance of carbon-based electrocatalysts. Significant research efforts should focus on
855 advancing reactor engineering, particularly for flow cell configurations and dual-PEM solid
856 electrolyte systems. These reactor designs must simultaneously address two critical challenges:
857 (1) corrosion resistance against both acidic/alkaline electrolytes and concentrated H₂O₂ (up to
858 10 wt%), and (2) maintenance of stable three-phase interfaces under industrial current densities
859 (>200 mA·cm⁻²). Innovative architectures incorporating corrosion-resistant materials (e.g.,
860 PTFE-coated titanium flow fields, stabilized carbon-PTFE gas diffusion electrodes) and
861 optimized hydrodynamics are crucial for achieving economically viable H₂O₂ electrosynthesis
862 at large scale. Furthermore, the H₂O₂ products are typically generated in a mixture, with solutes
863 in traditional liquid electrolytes ranging from acidic to alkaline pH. Extra separation processes



864 to recover pure H₂O₂ solutions are therefore required. Using a solid-state electrolyte can avoid
865 contamination of the product solution by extraneous ions.² Producing H₂O₂ in neutral solutions
866 offers practical advantages by avoiding pH-related complications, such as electrode degradation
867 or the need for neutralization steps. Seawater, as an abundant and naturally neutral electrolyte,
868 directly supports this goal by providing a sustainable medium for electrochemical H₂O₂
869 production via the 2e⁻ ORR pathway. The dissolved oxygen serves as a reactant for carbon-
870 based electrocatalysts, which have demonstrated high efficacy in neutral media. Moreover, the
871 use of seawater eliminates the costs and environmental impacts associated with synthetic pH
872 adjustments, enhancing both scalability and the sustainability of the process. However,
873 challenges such as chloride interference may compromise catalyst stability and selectivity,
874 necessitating the development of robust carbon-based materials and more in-depth mechanistic
875 studies in simulated seawater electrolytes to fully realize these benefits. Consequently,
876 exploring suitable and stable carbon-based catalysts and understanding the catalytic mechanism
877 in neutral simulated seawater electrolytes is an urgent and promising area of research.²¹²
878 Moreover, sustainable H₂O₂ production coupled to the high value added chemical synthesis
879 are worth exploring, such as oxidative valorization of glycerol²¹³ and cellulosic biomass
880 upgrading into valued formic acid.²¹⁴

881

882 **Acknowledgements**

883 This work was supported by financial aid from the National Natural Science Foundation of
884 China (Grant No. 22075126 and 52172187), the Start-up funding for Jinshan Distinguished
885 Professor of Jiangsu University, and the Jiangsu Provincial Senior Talent Program (Dengfeng).

886

887 **Conflicts of interest**

888 There are no conflicts to declare.

889



890 **References:**

- 891 1. R. Ciriminna, L. Albanese, F. Meneguzzo and M. Pagliaro, *ChemSusChem*, 2016, **9**,
892 3374-3381.
- 893 2. S. C. Perry, D. Pangotra, L. Vieira, L.-I. Csepei, V. Sieber, L. Wang, C. Ponce de León
894 and F. C. Walsh, *Nat. Rev. Chem.*, 2019, **3**, 442-458.
- 895 3. J. A. Dowling, K. Z. Rinaldi, T. H. Ruggles, S. J. Davis, M. Yuan, F. Tong, N. S. Lewis
896 and K. Caldeira, *Joule*, 2020, **4**, 1907-1928.
- 897 4. O. C. Esan, X. Shi, Z. Pan, Y. Liu, X. Huo, L. An and T. S. Zhao, *J. Power Sources*,
898 2022, **548**, 232114.
- 899 5. J. M. Campos-Martin, G. Blanco-Brieva and J. L. G. Fierro, *Angew. Chem. Int. Ed.*,
900 2006, **45**, 6962-6984.
- 901 6. A. G. Fink, R. S. Delima, A. R. Rousseau, C. Hunt, N. E. LeSage, A. Huang, M. Stolar
902 and C. P. Berlinguette, *Nat. Commun.*, 2024, **15**, 766.
- 903 7. S. J. Freakley, Q. He, J. H. Harrhy, L. Lu, D. A. Crole, D. J. Morgan, E. N. Ntainjua, J.
904 K. Edwards, A. F. Carley, A. Y. Borisevich, C. J. Kiely and G. J. Hutchings, *Science*,
905 2016, **351**, 965-968.
- 906 8. T. Ricciardulli, S. Gorthy, J. S. Adams, C. Thompson, A. M. Karim, M. Neurock and
907 D. W. Flaherty, *J. Am. Chem. Soc.*, 2021, **143**, 5445-5464.
- 908 9. Y. Zhang, C. Pan, G. Bian, J. Xu, Y. Dong, Y. Zhang, Y. Lou, W. Liu and Y. Zhu, *Nat.*
909 *Energy*, 2023, **8**, 361-371.
- 910 10. R. Liu, Y. Chen, H. Yu, M. Položij, Y. Guo, T. C. Sum, T. Heine and D. Jiang, *Nat.*
911 *Catal.*, 2024, **7**, 195-206.
- 912 11. Z. Teng, Q. Zhang, H. Yang, K. Kato, W. Yang, Y.-R. Lu, S. Liu, C. Wang, A.
913 Yamakata, C. Su, B. Liu and T. Ohno, *Nat. Catal.*, 2021, **4**, 374-384.
- 914 12. H. Tan, P. Zhou, M. Liu, Q. Zhang, F. Liu, H. Guo, Y. Zhou, Y. Chen, L. Zeng, L. Gu,
915 Z. Zheng, M. Tong and S. Guo, *Nat. Synth*, 2023, **2**, 557-563.
- 916 13. Y. Shiraishi, T. Takii, T. Hagi, S. Mori, Y. Kofuji, Y. Kitagawa, S. Tanaka, S. Ichikawa
917 and T. Hirai, *Nat. Mater.*, 2019, **18**, 985-993.
- 918 14. R. Pan, W. Lv, X. Ge, X. Huang, Q. Hu, K. Song, Q. Liu, H. Xie, B. Wu and J. Yuan,
919 *Adv. Funct. Mater.*, 2025, **35**, 2414193.
- 920 15. Y. Liu, L. Li, Z. Sang, H. Tan, N. Ye, C. Sun, Z. Sun, M. Luo and S. Guo, *Nat. Synth.*,
921 2025, **4**, 134-141.
- 922 16. P. Sun, Z. Mo, J. Zhang, G. Wu, Z. Miao, K. Zhong, Y. Wei, C. Jia, Z. Chen and H. Xu,
923 *Chem. Eng. J.*, 2023, **478**, 147337.
- 924 17. H. Jiang, L. Wang, X. Yu, L. Sun, J. Li, J. Yang and Q. Liu, *Chem. Eng. J.*, 2023, **466**,
925 143129.
- 926 18. C. Zhou, Y. Song, Z. Wang, J. Liu, P. Sun, Z. Mo, J. Yi and L. Zhai, *J. Environ. Chem.*
927 *Eng.*, 2023, **11**, 110138.
- 928 19. W. Wang, L. Wang, L. Sun, H. Jiang, Y. Liu, Q. Liu, X. She and H. Tang, *Chem. Eng.*
929 *J.*, 2023, **477**, 146945.
- 930 20. R. Chen, Z. Zhang, J. Wu, X. Chen, L. Wang, H. Yin, H. Li, J. Ding, H. Wan, G. Guan,
931 *Renew. Energy*, 2022, **197**, 943-952.
- 932 21. Z. Lu, G. Chen, S. Siahrostami, Z. Chen, K. Liu, J. Xie, L. Liao, T. Wu, D. Lin, Y. Liu,
933 T. F. Jaramillo, J. K. Nørskov and Y. Cui, *Nat. Catal.*, 2018, **1**, 156-162.
- 934 22. C. Xia, Y. Xia, P. Zhu, L. Fan and H. Wang, *Science*, 2019, **366**, 226-231.
- 935 23. E. Jung, H. Shin, B.-H. Lee, V. Efremov, S. Lee, H. S. Lee, J. Kim, W. Hooch Antink,
936 S. Park, K.-S. Lee, S.-P. Cho, J. S. Yoo, Y.-E. Sung and T. Hyeon, *Nat. Mater.*, 2020,
937 **19**, 436-442.
- 938 24. S. Siahrostami, A. Verdaguer-Casadevall, M. Karamad, D. Deiana, P. Malacrida, B.
939 Wickman, M. Escudero-Escribano, E. A. Paoli, R. Frydendal, T. W. Hansen, I.



- 940 Chorkendorff, I. E. L. Stephens and J. Rossmeisl, *Nat. Mater.*, 2013, **12**, 1137-1143. Open Access Article Online
DOI: 10.1039/D5MH00221D
- 941 25. Y. Jiang, P. Ni, C. Chen, Y. Lu, P. Yang, B. Kong, A. Fisher and X. Wang, *Adv. Energy*
- 942 *Mater.*, 2018, **8**, 1801909.
- 943 26. X. Sun, J. Yang, X. Zeng, L. Guo, C. Bie, Z. Wang, K. Sun, A. K. Sahu, M.
- 944 Tebyetekerwa, T. E. Rufford and X. Zhang, *Angew. Chem. Int. Ed.*, 2024, **63**,
- 945 e202414417.
- 946 27. D. Deng, J. Wang, M. Wang, Y. Wang, J. Jiang, Y. Chen, Y. Bai, Q. Wu and Y. Lei, *J.*
- 947 *Mater. Sci. Technol.*, 2025, **227**, 76-81.
- 948 28. L. Cui, B. Chen, D. Chen, C. He, Y. Liu, H. Zhang, J. Qiu, L. Liu, W. Jing and Z. Zhang,
- 949 *Nat. Commun.*, 2024, **15**, 10632.
- 950 29. J. Zhao, X. Zhang, J. Xu, W. Tang, Z. Lin Wang and F. Ru Fan, *Angew. Chem. Int. Ed.*,
- 951 2023, **62**, e202300604.
- 952 30. M. Ran, B. Du, W. Liu, Z. Liang, L. Liang, Y. Zhang, L. Zeng and M. Xing, *Proc. Natl.*
- 953 *Acad. Sci.*, 2024, **121**, e2317435121.
- 954 31. S. Li, X. Zhang, F. Yang, J. Zhang, W. Shi and F. Rosei, *Chem Catal.*, 2024, **4**, 100901.
- 955 32. S. Li, X. Liu, X. Zhang, Y. Liu, *Catalysts*, 2025, **15**, 157.
- 956 33. S. Li, X. Liu, X. Zhang, Y. Wang, S. Chen, Y. Liu and Y. Zhang, *Catalysts*, 2024, **14**,
- 957 159.
- 958 34. Q. Yang, Y. Gu, Y. Liu, X. Wang, S. Li, J. Zhang, W. Liu, L. Zhang and Y. Zhang,
- 959 *Chem. Commun.*, 2024, **60**, 13554-13557.
- 960 35. Y. Zhang, S. Li, J. Zhang, L.-D. Zhao, Y. Lin, W. Liu and F. Rosei, *Natl. Sci. Rev.*,
- 961 2024, **11**, nwae036.
- 962 36. S. Yang, A. Verdager-Casadevall, L. Arnarson, L. Silvioli, V. Čolić, R. Frydendal, J.
- 963 Rossmeisl, I. Chorkendorff, I. E. L. Stephens, *ACS Catal.*, 2018, **8**, 4064-4081.
- 964 37. S. Siahrostami, S. J. Villegas, A. H. Bagherzadeh Mostaghimi, S. Back, A. B. Farimani,
- 965 H. Wang, K. A. Persson, J. Montoya, *ACS Catal.*, 2020, **10**, 7495-7511.
- 966 38. J. Wang, D. Kim, J. H. Park, S. Ryu, M. Shokouhimehr and H. W. Jang, *Energy Fuels*,
- 967 2023, **37**, 17629-17651.
- 968 39. A. Yu, S. Liu and Y. Yang, *Chem. Commun.*, 2024, **60**, 5232-5244.
- 969 40. Y. Wang, G. I. N. Waterhouse, L. Shang and T. Zhang, *Adv. Energy Mater.*, 2021, **11**,
- 970 2003323.
- 971 41. J. S. Jirkovský, I. Panas, E. Ahlberg, M. Halasa, S. Romani and D. J. Schiffrin, *J. Am.*
- 972 *Chem. Soc.*, 2011, **133**, 19432-19441.
- 973 42. K. Gong, F. Du, Z. Xia, M. Durstock and L. Dai, *Science*, 2009, **323**, 760-764.
- 974 43. Q. Zhai, H. Huang, T. Lawson, Z. Xia, P. Giusto, M. Antonietti, M. Jaroniec, M.
- 975 Chhowalla, J.-B. Baek, Y. Liu, S. Qiao and L. Dai, *Adv. Mater.*, **36**, 2405664.
- 976 44. H. W. Kim, M. B. Ross, N. Kornienko, L. Zhang, J. Guo, P. Yang and B. D. McCloskey,
- 977 *Nat. Catal.*, 2018, **1**, 282-290.
- 978 45. J. Zhu, X. Xiao, K. Zheng, F. Li, G. Ma, H.-C. Yao, X. Wang and Y. Chen, *Carbon*,
- 979 2019, **153**, 6-11.
- 980 46. M. Niamlaem, C. Boonyuen, W. Sangthong, J. Limtrakul, D. Zigah, A. Kuhn and C.
- 981 Warakulwit, *Carbon*, 2020, **170**, 154-164.
- 982 47. J. Biemolt, K. van der Veen, N. J. Geels, G. Rothenberg and N. Yan, *Carbon*, 2019,
- 983 **155**, 643-649.
- 984 48. T.-N. Pham-Truong, T. Petenzi, C. Ranjan, H. Randriamahazaka and J. Ghilane, *Carbon*,
- 985 2018, **130**, 544-552.
- 986 49. A. R. Puente Santiago, O. Fernandez-Delgado, A. Gomez, M. A. Ahsan and L.
- 987 Echegoyen, *Angew. Chem. Int. Ed.*, 2021, **60**, 122-141.
- 988 50. Y. Liu, X. Quan, X. Fan, H. Wang and S. Chen, *Angew. Chem. Int. Edit.*, 2015, **54**,
- 989 6837-6841.
- 990 51. L. Jing, W. Wang, Q. Tian, Y. Kong, X. Ye, H. Yang, Q. Hu and C. He, *Angew. Chem.*



- 991 *Int. Edit.*, 2024, **63**, e202403023.
- 992 52. J. S. Lim, J. H. Kim, J. Woo, D. S. Baek, K. Ihm, T. J. Shin, Y. J. Sa and S. H. Joo,
993 *Chem*, 2021, **7**, 3114-3130.
- 994 53. L. Wei, Z. Dong, R. Chen, Q. Wu and J. Li, *Ionics*, 2022, **28**, 4045-4063.
- 995 54. Z.-y. Sang, F. Hou, S.-h. Wang and J. Liang, *Carbon*, 2022, **192**, 484.
- 996 55. Y.-Y. Yan, W.-J. Niu, W.-W. Zhao, R.-J. Li, E.-P. Feng, B.-X. Yu, B.-K. Chu and C.-
997 Y. Cai, *Adv. Energy Mater.*, 2024, **14**, 2303506.
- 998 56. H. He, S. Liu, Y. Liu, L. Zhou, H. Wen, R. Shen, H. Zhang, X. Guo, J. Jiang and B. Li,
999 *Green Chem.*, 2023, **25**, 9501-9542.
- 1000 57. Z. Deng, S. J. Choi, G. Li and X. Wang, *Chem. Soc. Rev.*, 2024, **53**, 8137-8181.
- 1001 58. H. He, S. Liu, Y. Liu, L. Zhou, H. Wen, R. Shen, H. Zhang, X. Guo, J. Jiang and B. Li,
1002 *Green Chem.*, 2023, **25**, 9501-9542
- 1003 59. X. Shi, S. Siahrostami, G.-L. Li, Y. Zhang, P. Chakthranont, F. Studt, T. F. Jaramillo,
1004 X. Zheng and J. K. Nørskov, *Nat. Commun.*, 2017, **8**, 701.
- 1005 60. L. Lin, L. Huang, C. Wu, Y. Gao, N. Miao, C. Wu, A. T. Marshall, Y. Zhao, J. Wang,
1006 J. Chen, S. Dou, G. G. Wallace and W. Huang, *Angew. Chem. Int. Ed.*, 2023, **62**,
1007 e202315182.
- 1008 61. J. Su, L. Jiang, B. Xiao, Z. Liu, H. Wang, Y. Zhu, J. Wang and X. Zhu, *Small*, 2023, **20**,
1009 2310317.
- 1010 62. R. Xie, C. Cheng, R. Wang, J. Li, E. Zhao, Y. Zhao, Y. Liu, J. Guo, P. Yin and T. Ling,
1011 *ACS Catal.*, 2024, **14**, 4471-4477.
- 1012 63. X. Luo, R. Zhu, L. Zhao, X. Gong, L. Zhang, L. Fan and Y. Liu, *Environ. Res.*, 2024,
1013 **251**, 118644.
- 1014 64. Luo, S.; Elouarzaki, K.; Xu, Z. J., Electrochemistry in Magnetic Fields. *Angew. Chem.*
1015 *Int. Ed.*, 2022, **61**, e202203564.
- 1016 65. X. Hu, Z. Sun, G. Mei, X. Zhao, B. Y. Xia and B. You, *Adv. Energy Mater.*, 2022, **12**,
1017 2201466.
- 1018 66. D. Kai, L. Jie, W. Yuanyuan, R. Yuchun, X. Zhaoquan, Z. Haiping, L. Lei, L. Qian, L.
1019 Yonglan, L. Tingshuai, M. A. Abdullah, L. Quan, M. Dongwei and S. Xuping, *Chem*
1020 *Catal.*, 2021, **1**, 1437-1448.
- 1021 67. S. Mavrikis, M. Göltz, S. C. Perry, F. Bogdan, P. K. Leung, S. Rosiwal, L. Wang and
1022 C. Ponce de León, *ACS Energy Lett.*, 2021, **6**, 2369-2377.
- 1023 68. Z. Chen, X. Liu, K. Wang, L. Yang, Y. Wang, X. Wang, S. Song, Z. Chen, *Adv. Funct.*
1024 *Mater.*, 2025, **35**, 2413243.
- 1025 69. Y. Liang, Y. Han, J.-s. Li, Wang, J. D. Liu, Q. Fan, *J. Energy Chem.*, 2022, **70**, 643-
1026 655.
- 1027 70. Y. Wang, Y. Xue, *ACS Appl. Nano Mater.*, 2023, **6**, 23565-23575.
- 1028 71. H. Zhang, Y. Zhao, Y. Li, G. Li, J. Li, F. Zhang, *ACS Appl. Energy Mater.*, 2020, **3**,
1029 705-714.
- 1030 72. S. Sun, J. Dang, K. Ji, Z. Shi, M. Chen, C. Zhang, S. Liu, *Renew. Sust. Energ. Rev.*,
1031 2023, **183**, 113538.
- 1032 73. Y. Jia and X. Yao, *Chem*, 2020, **6**, 548-550.
- 1033 74. Q. Chang, P. Zhang, A. H. B. Mostaghimi, X. Zhao, S. R. Denny, J. H. Lee, H. Gao, Y.
1034 Zhang, H. L. Xin, S. Siahrostami, J. G. Chen and Z. Chen, *Nat. Commun.*, 2020, **11**,
1035 2178.
- 1036 75. F. Y. Yu, Y. J. Zhou, H. Q. Tan, Y. G. Li and Z. H. Kang, *Adv. Energy Mater.*, 2023,
1037 **13**, 2300119.
- 1038 76. M. Deng, D. Wang and Y. Li, *Adv. Mater.*, 2024, **36**, 2314340.
- 1039 77. N. Ramaswamy, U. Tylus, Q. Jia, S. Mukerjee, *J. Am. Chem. Soc.*, 2013, **135**, 15443-
1040 15449.
- 1041 78. N. Ramaswamy, SMukerjee, *Phys. Chem. C*, 2011, **115**, 18015-18026.



- 1042 79. Y. Tang, B. L. Allen, D. R. Kauffman, A. Star, *J. Am. Chem. Soc.*, 2009, **131**, 13200-13201. Article Online
DOI: 10.1039/D5MH00221D
- 1043
- 1044 80. T.-P. Fellingner, F. Hasché, P. Strasser, M. Antonietti, *J. Am. Chem. Soc.*, 2012, **134**,
1045 4072-4075.
- 1046 81. Y. Pang, K. Wang, H. Xie, Y. Sun, M.-M. Titirici and G.-L. Chai, *ACS Catal.*, 2020,
1047 **10**, 7434-7442.
- 1048 82. Y. Xia, X. Zhao, C. Xia, Z.-Y. Wu, P. Zhu, J. Y. Kim, X. Bai, G. Gao, Y. Hu, J. Zhong,
1049 Y. Liu and H. Wang, *Nat. Commun.*, 2021, **12**, 4225.
- 1050 83. N. Wang, X. Zhao, R. Zhang, S. Yu, Z. H. Levell, C. Wang, S. Ma, P. Zou, L. Han, J.
1051 Qin, L. Ma, Y. Liu and H. L. Xin, *ACS Catal.*, 2022, **12**, 4156-4164.
- 1052 84. Q. Tian, L. Jing, H. Du, Y. Yin, X. Cheng, J. Xu, J. Chen, Z. Liu, J. Wan, J. Liu and J.
1053 Yang, *Nat. Commun.*, 2024, **15**, 983.
- 1054 85. L. Yang, H. Cheng, H. Li, G. Sun, S. Liu, T. Ma and L. Zhang, *Adv. Mater.*, 2024, **36**,
1055 2406957.
- 1056 86. Q. Tian, L. Jing, Y. Yin, Z. Liang, H. Du, L. Yang, X. Cheng, D. Zuo, C. Tang, Z. Liu,
1057 J. Liu, J. Wan and J. Yang, *Nano Lett.*, 2024, **24**, 1650-1659.
- 1058 87. C. Du, P. Li, Z. Zhuang, Z. Fang, S. He, L. Feng and W. Chen, *Coordin. Chem. Rev.*,
1059 2022, **466**, 214604.
- 1060 88. L. Kořená, V. Slovák, G. Zelenková and T. Zelenka, *Carbon*, 2023, **206**, 303-313.
- 1061 89. A. Wang, Y. Ma and D. Zhao, *ACS Nano*, 2024, **18**, 22829-22854.
- 1062 90. L. Jing, Q. Tian, W. Wang, X. Li, Q. Hu, H. Yang and C. He, *Adv. Energy Mater.*, 2024,
1063 **14**, 2304418.
- 1064 91. Y. Hu, J. Zhang, T. Shen, Z. Li, K. Chen, Y. Lu, J. Zhang and D. Wang, *ACS Appl.*
1065 *Mater. Interfaces*, 2021, **13**, 29551-29557.
- 1066 92. J. Xi, S. Yang, L. Silvioli, S. Cao, P. Liu, Q. Chen, Y. Zhao, H. Sun, J. N. Hansen, J.-P.
1067 B. Haraldsted, J. Kibsgaard, J. Rossmeisl, S. Bals, S. Wang and I. Chorkendorff, *J.*
1068 *Catal.*, 2021, **393**, 313-323.
- 1069 93. C. Qi, W. Bao, J. Xu, Y. Li, F. Xu, M. Li, L. Wang, W. Jiang, P. Qiu and W. Luo,
1070 *Angew. Chem. Int. Ed.*, 2025, e202500177. doi: 10.1002/anie.202500177.
- 1071 94. W. Zhu, Z. Chen, Y. Pan, R. Dai, Y. Wu, Z. Zhuang, D. Wang, Q. Peng, C. Chen and
1072 Y. Li, *Adv. Mater.*, 2019, **31**, 1800426.
- 1073 95. Z. Yu, N. Ji, X. Li, R. Zhang, Y. Qiao, J. Xiong, J. Liu and X. Lu, *Angew. Chem. Int.*
1074 *Ed.*, 2023, **62**, e202213612.
- 1075 96. X. Tang, Y. Wei, W. Zhai, Y. Wu, T. Hu, K. Yuan and Y. Chen, *Adv. Mater.*, 2023, **35**,
1076 2208942.
- 1077 97. Y. Bu, Y. Wang, G.-F. Han, Y. Zhao, X. Ge, F. Li, Z. Zhang, Q. Zhong and J.-B. Baek,
1078 *Adv. Mater.*, 2021, **33**, 2103266.
- 1079 98. J. Zhu and S. Mu, *Adv. Funct. Mater.*, 2020, **30**, 2001097.
- 1080 99. L. Jing, Q. Tian, X. Li, J. Sun, W. Wang, H. Yang, X. Chai, Q. Hu and C. He, *Adv.*
1081 *Funct. Mater.*, 2023, **33**, 2305795.
- 1082 100. Z. Mou, Y. Mu, L. Liu, D. Cao, S. Chen, W. Yan, H. Zhou, T.-S. Chan, L.-Y. Chang
1083 and X. Fan, *Small*, 2024, **20**, 2400564.
- 1084 101. C. Zhang, C. Wu, L. Wang and G. Liu, *ACS Appl. Mater. Interfaces*, 2023, **15**, 838-847.
- 1085 102. J. Zhu, Y. Huang, W. Mei, C. Zhao, C. Zhang, J. Zhang, I. S. Amiinu and S. Mu, *Angew.*
1086 *Chem. Int. Ed.*, 2019, **58**, 3859-3864.
- 1087 103. C. Zhang, W. Shen, K. Guo, M. Xiong, J. Zhang and X. Lu, *J. Am. Chem. Soc.*, 2023,
1088 **145**, 11589-11598.
- 1089 104. L. Lin, L. Huang, C. Wu, Y. Gao, N. Miao, C. Wu, A. T. Marshall, Y. Zhao, J. Wang,
1090 J. Chen, S. Dou, G. G. Wallace and W. Huang, *Angew. Chem. Int. Ed.*, 2023, **62**,
1091 e202315182.
- 1092 105. D. San Roman, D. Krishnamurthy, R. Garg, H. Hafiz, M. Lamparski, N. T. Nuhfer, V.



- 1093 Meunier, V. Viswanathan and T. Cohen-Karni, *ACS Catal.*, 2020, **10**, 1993-2008. View Article Online
DOI: 10.1039/D5MH00221D
- 1094 106. Y. J. Sa, J. H. Kim and S. H. Joo, *Angew. Chem. Int. Ed.*, 2019, **58**, 1100-1105.
- 1095 107. F. She, Z. Guo, F. Liu, Z. Yu, J. Chen, Y. Fan, Y. Lei, Y. Chen, H. Li and L. Wei, *ACS Catal.*, 2024, **14**, 10928-10938.
- 1096 108. X. Wang, C. Han, Y. Han, R. Huang, H. Sun, P. Guo, X. Liu, M. Huang, Y. Chen, H. Wu, J. Zhang, X. Yan, Z. Mao, A. Du, Y. Jia and L. Wang, *Small*, 2024, **20**, 2401447.
- 1097 109. W. Shen, C. Zhang, M. Alomar, Z. Du, Z. Yang, J. Wang, G. Xu, J. Zhang, J. Lv and X. Lu, *Nano Res.*, 2024, **17**, 1217-1224.
- 1098 110. M. Fan, Z. Wang, K. Sun, A. Wang, Y. Zhao, Q. Yuan, R. Wang, J. Raj, J. Wu, J. Jiang and L. Wang, *Adv. Mater.*, 2023, **35**, 2209086.
- 1103 111. J. W. Choi, A. Byeon, S. Kim, C.-K. Hwang, W. Zhang, J. Lee, W. C. Yun, S. Y. Paek, J. H. Kim, G. Jeong, S. Y. Lee, J. Moon, S. S. Han, J. W. Lee and J. M. Kim, *Adv. Mater.*, 2025, doi: 10.1002/adma.202415712.
- 1106 112. N. Wang, S. Ma, R. Zhang, L. Wang, Y. Wang, L. Yang, J. Li, F. Guan, J. Duan and B. Hou, *Adv. Sci.*, 2023, **10**, 2302446.
- 1108 113. Z. Xing, K. Shi, Z. S. Parsons and X. Feng, *ACS Catal.*, 2023, **13**, 2780-2789.
- 1109 114. L. Xie, C. Liang, Y. Wu, K. Wang, W. Hou, H. Guo, Z. Wang, Y. M. Lam, Z. Liu and L. Wang, *Small*, **20**, 2401253.
- 1111 115. W. Shen, C. Zhang, X. Wang, Y. Huang, Z. Du, M. Alomar, J. Wang, J. Lv, J. Zhang and X. Lu, *ACS Materials Lett.*, 2024, **6**, 17-26.
- 1113 116. H. Jiang, Y. Wang, J. Hao, Y. Liu, W. Li and J. Li, *Carbon*, 2017, **122**, 64-73.
- 1114 117. Y. Wu, Z. Gao, Y. Feng, Q. Cui, C. Du, C. Yu, L. Liang, W. Zhao, J. Feng, J. Sun, R. Yang and J. Sun, *Appl. Catal. B-Environ.*, 2021, **298**, 120572.
- 1115 118. C. Ma, Q. Hao, J. Hou, A. Liu and X. Xiang, *Carbon Res.*, 2024, **3**, 5.
- 1117 119. G.-F. Han, F. Li, W. Zou, M. Karamad, J.-P. Jeon, S.-W. Kim, S.-J. Kim, Y. Bu, Z. Fu, Y. Lu, S. Siahrostami and J.-B. Baek, *Nat. Commun.*, 2020, **11**, 2209.
- 1119 120. X. Shen, Z. Wang, H. Guo, Z. Lei, Z. Liu and L. Wang, *Small*, 2023, **19**, 2303156.
- 1120 121. Q. Wu, H. Zou, X. Mao, J. He, Y. Shi, S. Chen, X. Yan, L. Wu, C. Lang, B. Zhang, L. Song, X. Wang, A. Du, Q. Li, Y. Jia, J. Chen and X. Yao, *Nat. Commun.*, 2023, **14**, 6275.
- 1123 122. J. Qu, G. Long, L. Luo, Y. Yang, W. Fan and F. Zhang, *Small*, 2024, **20**, 2400695.
- 1124 123. X. Wen, X. Zhang, M. Wang, C. Yuan, J. Lang, X. Li, H. Wei, D. Mandler and M. Long, *Appl. Catal. B-Environ.*, 2024, **342**, 123437.
- 1125 124. G. Alemany-Molina, J. Fernández-Catalá, W. Cao, E. Morallón and D. Cazorla-Amorós, *Mater. Today Chem.*, 2024, **35**, 101858.
- 1127 125. A. Zhang, Y. Liu, J. Wu, J. Zhu, S. Cheng, Y. Wang, Y. Hao and S. Zeng, *Chem. Eng. J.*, 2023, **454**, 140317.
- 1128 126. A. B. Trench, J. Paulo C. Moura, V. S. Antonin, C. Machado Fernandes, L. Liu and M. C. Santos, *Adv. Powder Technol.*, 2024, **35**, 104404.
- 1131 127. M. A. Rashed, M. Faisal, F. A. Harraz, M. Jalalah, M. Alsaieri and S. A. Alsareii, *J. Electrochem. Soc.*, 2021, **168**, 027512.
- 1132 128. B. Yu, J. Diniz, K. Lofgren, Q. Liu, R. Mercado, F. Nichols, S. R. J. Oliver and S. Chen, *ACS Sustain. Chem. Eng.*, 2022, **10**, 15501-15507.
- 1134 129. C. Guo, Y. Ruan, S. Zhang, L. Kan, H. Bian, F. Rong, L. He, D. Li, M. Du and Z. Zhang, *Chem. Eng. J.*, 2023, **466**, 143033.
- 1136 130. N. Cheng, S. Stambula, D. Wang, M. N. Banis, J. Liu, A. Riese, B. Xiao, R. Li, T.-K. Sham, L.-M. Liu, G. A. Botton and X. Sun, *Nat. Commun.*, 2016, **7**, 13638.
- 1138 131. Q. Chang, P. Zhang, A. H. B. Mostaghimi, X. Zhao, S. R. Denny, J. H. Lee, H. Gao, Y. Zhang, H. L. Xin, S. Siahrostami, J. G. Chen and Z. Chen, *Nat. Commun.*, 2020, **11**, 2178.
- 1140 132. C. Jing, J. Ding, P. Jia, M. Jin, L. Zhou, X. Liu, J. Luo and S. Dai, *Carbon Energ.*, 2024,



- 1144 6, e581.
- 1145 133. G. Wei, Y. Li, X. Liu, J. Huang, M. Liu, D. Luan, S. Gao and X. W. Lou, *Angew. Chem. Int. Ed.*, 2023, **62**, e202313914.
- 1146 134. C. Xiao, L. Cheng, Y. Zhu, G. Wang, L. Chen, Y. Wang, R. Chen, Y. Li and C. Li, *Angew. Chem. Int. Ed.*, 2022, **61**, e202206544.
- 1147 135. M. Deng, D. Wang and Y. Li, *Adv. Mater.*, 2024, **36**, 2314340.
- 1148 136. Y.-X. Du, Q. Yang, W.-T. Lu, Q.-Y. Guan, F.-F. Cao and G. Zhang, *Adv. Funct. Mater.*, 2023, **33**, 2300895.
- 1149 137. M. Song, W. Liu, J. Zhang, C. Zhang, X. Huang and D. Wang, *Adv. Funct. Mater.*, 2023, **33**, 2212087.
- 1150 138. H. Gong, Z. Wei, Z. Gong, J. Liu, G. Ye, M. Yan, J. Dong, C. Allen, J. Liu, K. Huang, R. Liu, G. He, S. Zhao and H. Fei, *Adv. Funct. Mater.*, 2022, **32**, 2106886.
- 1151 139. C.-K. Hwang, S. Kim, K. R. Yoon, T. T. Le, C. V. Hoang, J. W. Choi, W. Zhang, S. Y. Paek, C. H. Lee, J. H. Lee, K. H. Chae, S. Jeong, S. Y. Lee, B.-K. Ju, S. H. Kim, S. S. Han and J. M. Kim, *Carbon Energ.*, 2024, **6**, e582.
- 1152 140. S. Zhang, Z. Tao, M. Xu, L. Kan, C. Guo, J. Liu, L. He, M. Du and Z. Zhang, *Small*, 2024, **20**, 2310468.
- 1153 141. C. Tang, L. Chen, H. Li, L. Li, Y. Jiao, Y. Zheng, H. Xu, K. Davey and S.-Z. Qiao, *J. Am. Chem. Soc.*, 2021, **143**, 7819-7827.
- 1154 142. H. Xu, S. Zhang, X. Zhang, M. Xu, M. Han, L. R. Zheng, Y. Zhang, G. Wang, H. Zhang and H. Zhao, *Angew. Chem. Int. Ed.*, 2023, **62**, e202314414.
- 1155 143. L.-Y. Dong, J.-S. Wang, T.-Y. Li, T. Wu, X. Hu, Y.-T. Wu, M.-Y. Zhu, G.-P. Hao and A.-H. Lu, *Angew. Chem. Int. Ed.*, 2024, **63**, e202317660.
- 1156 144. F. Zhang, Y. Zhu, C. Tang, Y. Chen, B. Qian, Z. Hu, Y.-C. Chang, C.-W. Pao, Q. Lin, S. A. Kazemi, Y. Wang, L. Zhang, X. Zhang and H. Wang, *Adv. Funct. Mater.*, 2022, **32**, 2110224.
- 1157 145. H. Yang, N. Lu, J. Zhang, R. Wang, S. Tian, M. Wang, Z. Wang, K. Tao, F. Ma and S. Peng, *Carbon Energ.*, 2023, **5**, e337.
- 1158 146. J. H. Kim, D. Shin, J. Lee, D. S. Baek, T. J. Shin, Y.-T. Kim, H. Y. Jeong, J. H. Kwak, H. Kim and S. H. Joo, *ACS Nano*, 2020, **14**, 1990-2001.
- 1159 147. X. Zhou, Y. Min, C. Zhao, C. Chen, M.-K. Ke, S.-L. Xu, J.-J. Chen, Y. Wu and H.-Q. Yu, *Nat. Commun.*, 2024, **15**, 193.
- 1160 148. Y. Gu, Y. Tan, H. Tan, Y. Han, D. Cheng, F. Lin, Z. Qian, L. Zeng, S. Zhang, R. Zeng, Y. Liu, H. Guo, M. Luo and S. Guo, *Nat. Synth.*, 2025, **4**, 857.
- 1161 149. E. Zhang, L. Tao, J. An, J. Zhang, L. Meng, X. Zheng, Y. Wang, N. Li, S. Du, J. Zhang, D. Wang and Y. Li, *Angew. Chem. Int. Ed.*, 2022, **61**, e202117347.
- 1162 150. J. Gao, H. b. Yang, X. Huang, S.-F. Hung, W. Cai, C. Jia, S. Miao, H. M. Chen, X. Yang, Y. Huang, T. Zhang and B. Liu, *Chem*, 2020, **6**, 658-674.
- 1163 151. J. Du, G. Han, W. Zhang, L. Li, Y. Yan, Y. Shi, X. Zhang, L. Geng, Z. Wang, Y. Xiong, G. Yin and C. Du, *Nat. Commun.*, 2023, **14**, 4766.
- 1164 152. A. I. M. Albashir, X. Lu, X. Dai, W. Qi, *Commun. Chem.*, 2024, **7**, 111.
- 1165 153. M. Yang, W. Song, C. Chen, X. Yang, Z. Zhuang, H. Zhang, F. Wang, L. Yu, *Adv. Mater.*, 2025, 2416401, doi.org/10.1002/adma.202416401.
- 1166 154. C. Liu, H. Tong, P. Wang, P. Huang, Z. Yang, R. Huang and G. Zhou, *Chem. Eng. J.*, 2023, **476**, 146573.
- 1167 155. Y. Wang, Y. Zhou, Y. Feng and X. Y. Yu, *Adv. Funct. Mater.*, 2022, **32**, 2110734.
- 1168 156. T. C. Nagaiah, D. Schäfer, W. Schuhmann, N. Dimcheva, *Anal. Chem.* 2013, **85**, 7897-7903.
- 1169 157. Y. Chang, J. Yang, M. Zhang, M. Yue, W. Wang, J. Li, J. Wang, K. Song, Y. Liu, Y. Zuo, R. Xing, *J. Alloy. Compd.*, 2024, **1005**, 176091.
- 1170 158. R. Gao, L. Pan, Z. Li, C. Shi, Y. Yao, X. Zhang, J.-J. Zou, *Adv. Funct. Mater.*, 2020,

View Article Online
DOI: 10.1039/D5MH00221D

- 1195 **30**, 1910539.
- 1196 159. Y. Zhang, M. Wang, W. Zhu, M. Fang, M. Ma, F. Liao, H. Yang, T. Cheng, C.-W.
- 1197 Pao, Y.-C. Chang, Z. Hu, Q. Shao, M. Shao, Z. Kang, *Angew. Chem. Int. Ed.*, 2023, **62**,
- 1198 e202218924.
- 1199 160. H. Li, P. Wen, D. S. Itanze, Z. D. Hood, S. Adhikari, C. Lu, X. Ma, C. Dun, L. Jiang,
- 1200 D. L. Carroll, Y. Qiu, S. M. Geyer, *Nat. Commun.*, 2020, **11**, 3928.
- 1201 161. R. Shen, W. Chen, Q. Peng, S. Lu, L. Zheng, X. Cao, Y. Wang, W. Zhu, J. Zhang,
- 1202 Z. Zhuang, C. Chen, D. Wang, Y. Li, *Chem*, 2019, **5**, 2099-2110.
- 1203 162. X.-D. Zhu, Q. Zhang, X. Yang, Y. Wang, J. Wu, J. Gao, J.-J. Zou, G. Wu, Y.-C.
- 1204 Zhang, *SusMat*, 2023, **3**, 334-344.
- 1205 163. H. Xu, S. Zhang, X. Zhang, M. Xu, M. Han, L. R. Zheng, Y. Zhang, G. Wang, H. Zhang
- 1206 and H. Zhao, *Angew. Chem. Int. Edit.*, 2023, **62**, e202314414.
- 1207 164. Y. Long, J. Lin, F. Ye, W. Liu, D. Wang, Q. Cheng, R. Paul, D. Cheng, B. Mao, R. Yan,
- 1208 L. Zhao, D. Liu, F. Liu and C. Hu, *Adv. Mater.*, 2023, **35**, 2303905.
- 1209 165. A. Byeon, J. W. Choi, H. W. Lee, W. C. Yun, W. Zhang, C.-K. Hwang, S. Y. Lee, S. S.
- 1210 Han, J. M. Kim and J. W. Lee, *Appl. Catal. B-Environ.*, 2023, **329**, 122557.
- 1211 166. M. Wang, N. Zhang, Y. Feng, Z. Hu, Q. Shao, X. Huang, *Angew. Chem. Int. Ed.*, 2020,
- 1212 **59**, 14373-14377.
- 1213 167. Y. Wu, Y. Zhao, Q. Yuan, H. Sun, A. Wang, K. Sun, G. I. N. Waterhouse, Z. Wang,
- 1214 J. Wu, J. Jiang, M. Fan, *Nat. Commun.* 2024, **15**, 10843.
- 1215 168. Q. Tian, L. Jing, H. Du, Y. Yin, X. Cheng, J. Xu, J. Chen, Z. Liu, J. Wan, J. Liu and J.
- 1216 Yang, *Nat. Commun.*, 2024, **15**, 983.
- 1217 169. L. June Sung, K. Jae Hyung, W. Jinwoo, B. Du San, I. Kyuwook, S. Tae Joo, S. Young
- 1218 Jin and J. Sang Hoon, *Chem*, 2021, **7**, 3114-3130.
- 1219 170. Y. J. Sa, J. H. Kim and S. H. Joo, *Angew. Chem. Int. Ed.*, 2018, **58**, 1100-1105.
- 1220 171. K. Dong, J. Liang, Y. Wang, Z. Xu, Q. Liu, Y. Luo, T. Li, L. Li, X. Shi, A. M. Asiri, Q.
- 1221 Li, D. Ma and X. Sun, *Angew. Chem. Int. Ed.*, 2021, **60**, 10583-10587.
- 1222 172. L. Liu, L. Kang, A. Chutia, J. Feng, M. Michalska, P. Ferrer, D. C. Grinter, G. Held, Y.
- 1223 Tan, F. Zhao, F. Guo, D. G. Hopkinson, C. S. Allen, Y. Hou, J. Gu, I. Papakonstantinou,
- 1224 P. R. Shearing, D. J. L. Brett, I. P. Parkin and G. He, *Angew. Chem. Int. Ed.*, 2023, **62**,
- 1225 e202303525.
- 1226 173. D. Zhiping and W. Xiaolei, *Nano Res.*, 2022, **15**, 4599-4605.
- 1227 174. L. Jing, Q. Tian, X. Li, J. Sun, W. Wang, H. Yang, X. Chai, Q. Hu and C. He, *Adv.*
- 1228 *Funct. Mater.*, 2023, **33**, 2305795.
- 1229 175. K. H. Koh, A. H. Bagherzadeh Mostaghimi, Q. Chang, Y. J. Kim, S. Siahrostami, T. H.
- 1230 Han and Z. Chen, *EcoMat*, 2023, **5**, e12266.
- 1231 176. F. She, Z. Guo, F. Liu, Z. Yu, J. Chen, Y. Fan, Y. Lei, Y. Chen, H. Li and L. Wei, *ACS*
- 1232 *Catal.*, 2024, **14**, 10928-10938.
- 1233 177. L. Xie, C. Liang, Y. Wu, K. Wang, W. Hou, H. Guo, Z. Wang, Y. M. Lam, Z. Liu and
- 1234 L. Wang, *Small*, 2024, **20**, e2401253.
- 1235 178. Q. Wu, H. Zou, X. Mao, J. He, Y. Shi, S. Chen, X. Yan, L. Wu, C. Lang, B. Zhang, L.
- 1236 Song, X. Wang, A. Du, Q. Li, Y. Jia, J. Chen and X. Yao, *Nat. Commun.*, 2023, **14**,
- 1237 6275.
- 1238 179. P. Chakthranont, S. Nitrathorn, S. Thongratkaew, P. Khemthong, H. Nakajima, R.
- 1239 Supruangnet, T. Butburee, N. Sano and K. Faungnawakij, *ACS Appl. Energy Mater.*,
- 1240 2021, **4**, 12436-12447.
- 1241 180. W. Shen, C. Zhang, M. Alomar, Z. Du, Z. Yang, J. Wang, G. Xu, J. Zhang, J. Lv and
- 1242 X. Lu, *Nano Res.*, 2023, **17**, 1217-1224.
- 1243 181. Y. Xia, X. Zhao, C. Xia, Z.-Y. Wu, P. Zhu, J. Y. T. Kim, X. Bai, G. Gao, Y. Hu, J.
- 1244 Zhong, Y. Liu and H. Wang, *Nat. Commun.*, 2021, **12**, 4225.
- 1245 182. Y. Hu, J. Zhang, T. Shen, Z. Li, K. Chen, Y. Lu, J. Zhang and D. Wang, *ACS Appl.*



- 1246 *Mater. Interfaces*, 2021, **13**, 29551-29557.
- 1247 183. L. Han, Y. Sun, S. Li, C. Cheng, C. E. Halbig, P. Feicht, J. L. Hübner, P. Strasser and
1248 S. Eigler, *ACS Catal.*, 2019, **9**, 1283-1288.
- 1249 184. C. Zhang, W. Shen, K. Guo, M. Xiong, J. Zhang and X. Lu, *J. Am. Chem. Soc.*, 2023,
1250 **145**, 11589-11598.
- 1251 185. N. Wang, S. Ma, R. Zhang, L. Wang, Y. Wang, L. Yang, J. Li, F. Guan, J. Duan and B.
1252 Hou, *Adv. Sci.*, 2023, **10**, 2302446.
- 1253 186. L. Jing, Q. Tian, W. Wang, X. Li, Q. Hu, H. Yang and C. He, *Adv. Energy Mater.*, 2024,
1254 **14**, 2304418.
- 1255 187. Y. Liu, S. Liu, J. Jiang, X. Wei, K. Zhao, R. Shen, X. Wang, M. Wei, Y. Wang, H.
1256 Pang, B. Li, *Adv. Mater.*, 2025, 2502197. doi.org/10.1002/adma.202502197.
- 1257 188. H. Gong, L. Wei, S. Chen, Z. Chen, T. F. Jaramillo and Z. Bao, *Nano Res.*, 2023, **16**,
1258 11556-11563.
- 1259 189. K.-H. Wu, D. Wang, X. Lu, X. Zhang, Z. Xie, Y. Liu, B.-J. Su, J.-M. Chen, D.-S. Su,
1260 W. Qi and S. Guo, *Chem*, 2020, **6**, 1443-1458.
- 1261 190. C. Yang, F. Sun, Z. Qu, X. Li, W. Zhou, J. Gao, *ACS Energy Lett.* 2022, **7**, 4398-4407
- 1262 191. M. Fan, Z. Wang, K. Sun, A. Wang, Y. Zhao, Q. Yuan, R. Wang, J. Raj, J. Wu, J. Jiang
1263 and L. Wang, *Adv. Mater.*, 2023, **35**, 2209086.
- 1264 192. X. Zhou, Y. Min, C. Zhao, C. Chen, M.-K. Ke, S.-L. Xu, J.-J. Chen, Y. Wu and H.-Q.
1265 Yu, *Nat. Commun.*, 2024, **15**, 193.
- 1266 193. E. Zhang, L. Tao, J. An, J. Zhang, L. Meng, X. Zheng, Y. Wang, N. Li, S. Du, J. Zhang,
1267 D. Wang and Y. Li, *Angew. Chem. Int. Ed.*, 2022, **61**, e202117347.
- 1268 194. H. Yang, N. Lu, J. Zhang, R. Wang, S. Tian, M. Wang, Z. Wang, K. Tao, F. Ma, Peng,
1269 S., *Carbon Energy*, 2023, **5**, e337.
- 1270 195. J. Shen, Y. Wen, H. Jiang, S. Yu, C. Dong, Y. Fan, B. Liu and C. Li, *J. Phys. Chem.C*,
1271 **2022**, **126**, 10388-10398.
- 1272 196. L. Yang, H. Cheng, H. Li, G. Sun, S. Liu, T. Ma and L. Zhang, *Adv. Mater.*, 2024, **36**,
1273 2406957.
- 1274 197. S. Zhang, Z. Tao, M. Xu, L. Kan, C. Guo, J. Liu, L. He, M. Du and Z. Zhang, *Small*,
1275 **2024**, **20**, 2310468.
- 1276 198. H. Gong, Z. Wei, Z. Gong, J. Liu, G. Ye, M. Yan, J. Dong, C. Allen, J. Liu, K. Huang,
1277 R. Liu, G. He, S. Zhao and H. Fei, *Adv. Funct. Mater.*, 2021, **32**, 2106886.
- 1278 199. H. Gong, Z. Gong, J. Liu, G. Ye and H. Fei, *Adv. Funct. Mater.*, 2024, **34**, 2316438.
- 1279 200. W. Liu, R. Chen, Z. Sang, Z. Li, J. Nie, L. Yin, F. Hou and J. Liang, *Adv. Mater.*, 2024,
1280 **36**, 2406403.
- 1281 201. E. A. Moges, C.-Y. Chang, W.-H. Huang, F. T. Angerasa, K. Lakshmanan, T. M. Hagos,
1282 H. G. Edao, W. B. Dilebo, C.-W. Pao, M.-C. Tsai, W.-N. Su and B. J. Hwang, *J. Am.*
1283 *Chem. Soc.*, 2023, **12**, 4156-4164.
- 1284 202. N. Wang, X. Zhao, R. Zhang, S. Yu, Z. H. Levell, C. Wang, S. Ma, P. Zou, L. Han, J.
1285 Qin, L. Ma, Y. Liu and H. L. Xin, *ACS Catal.*, 2022, **12**, 4156-4164.
- 1286 203. G. Wei, Y. Li, X. Liu, J. Huang, M. Liu, D. Luan, S. Gao and X. W. D. Lou, *Angew.*
1287 *Chem. Int. Ed.*, 2023, **62**, e202313914.
- 1288 204. C. K. Hwang, S. Kim, K. R. Yoon, T. T. Le, C. V. Hoang, J. W. Choi, W. Zhang, S. Y.
1289 Paek, C. H. Lee, J. H. Lee, K. H. Chae, S. Jeong, S. Y. Lee, B. K. Ju, S. H. Kim, S. S.
1290 Han and J. M. Kim, *Carbon Energ.*, 2024, **6**, e582.
- 1291 205. F. Zhang, Y. Zhu, C. Tang, Y. Chen, B. Qian, Z. Hu, Y. C. Chang, C. W. Pao, Q. Lin,
1292 S. A. Kazemi, Y. Wang, L. Zhang, X. Zhang and H. Wang, *Adv. Funct. Mater.*, 2021,
1293 **32**, 2110224.
- 1294 206. C. Zhang, C. Wu, L. Wang and G. Liu, *ACS Appl. Mater. Interfaces*, 2023, **15**, 838-847.
- 1295 207. Y. Wang, Y. Zhou, Y. Feng, X. Y. Yu, *Adv. Funct. Mater.*, 2022, **32**, 2110734.
- 1296 208. C. Xiao, L. Cheng, Y. Zhu, G. Wang, L. Chen, Y. Wang, R. Chen, Y. Li and C. Li,

View Article Online
DOI: 10.1039/D5MH00221D

- 1297 *Angew. Chem. Int. Ed.*, 2022, **61**, e202206544.
- 1298 209. W. Yuhan, G. Zhixiao, F. Yiran, C. Qiannan, D. Cuiwei, Y. Chongfei, L. Liang, Z. Wen,
1299 F. Jinglan, S. Jianhui, Y. Ruizhi and S. Jingyu, *Appl. Catal. B-Environ.*, 2021, **298**,
1300 120572.
- 1301 210. C. Yang, F. Sun, Z. Qu, X. Li, W. Zhou and J. Gao, *ACS Energy Lett.*, 2022, **7**, 4398-
1302 4407.
- 1303 211. Y. Xia, P. Zhu, Y. Yang, C. Qiu, H. Wang, *ACS Catal.*, 2025, **15**, 4560-4569.
- 1304 212. J. Wang, J. Li, Z. Li, J. Wu, H. Si, Y. Wu, Z. Guo, X. Wang, F. Liao, H. Huang, M.
1305 Shao, Y. Liu and Z. Kang, *Nano Res.*, 2024, **17**, 5956-5964.
- 1306 213. D. Oh, S. W. Hwang, D. Y. Kim, J. E. Matthews, J. Lee, J. E. A. Acosta, S.-W. Lee,
1307 Y. Xu, A. Cho, D. U. Lee, T. F. Jaramillo, D.-H. Seo, J.-W. Jang, *Nat. Synth.*, 2025,
1308 doi.org/10.1038/s44160-025-00774-y.
- 1309 214. K. Yu, S. Guan, W. Zhang, W. Zhang, Y. Meng, H. Lin, Q. Gao, *Angew. Chem. Int.*
1310 *Edit.*, 2025, e202502383. doi.org/10.1002/anie.202502383.

View Article Online

DOI: 10.1039/D5MH00221D

